M 2024

U.PORTO
FEUP FACULDADE DE ENGENHARIA
UNIVERSIDADE DO PORTO

SLOT-DIE COATING FOR EFFICIENT AND SCALABLE INVERTED PEROVSKITE SOLAR CELLS IN AMBIENT AIR

LUÍS FILIPE SILVA DOS SANTOS
MASTER THESIS IN CHEMICAL ENGINEERING
PRESENTED TO THE FACULTY OF ENGINEERING
OF THE UNIVERSITY OF PORTO

Master in Chemical Engineering

Slot-die coating for efficient and scalable inverted Perovskite Solar Cells in ambient air

Master Thesis

of

Luís Filipe Silva dos Santos

Developed within the course of dissertation

held in

LEPABE



Supervisor: **Prof. Luísa Andrade**

Joint supervisor: **Dr. Vera Duarte**





July 2024

Acknowledgment

I would like to express my gratitude to everyone who supported me throughout my master's thesis. This work would not have been possible without the help and collaboration of several people and institutions.

Firstly, I would like to thank my supervisor, Dr. Luísa Andrade, for her orientation, patience and support throughout the process. Her suggestions and constructive criticism were fundamental to the development of this work.

I would like to thank my joint supervisor, Dr. Vera Duarte, for her valuable input and support in the laboratory. Her insights and knowledge were essential to the success of this work.

I would like to thank all the researchers and PhD students who work at UPTEC for the affable environment and help throughout this work.

I want to thank my friends, who were always ready to help and encourage me in the most challenging moments.

I would like to thank my parents and brothers for their love, support, and sacrifices over the years. This work wouldn't be possible without their understanding, encouragement and motivation.

I would also like to thank LEPABE - Laboratory for Process Engineering Environment, Biotechnology and Energy for providing the resources and environment needed to carry out this research.

Finally, I would like to thank all those who, in one way or another, contributed to the realization of this work and have not been mentioned individually.

This work was supported by: InPSC project (PTDC/EQU-EQU/4193/2021) with DOI 10.54499/PTDC/EQU-EQU/4193/2021 (https://doi.org/10.54499/PTDC/EQU-EQU/4193/2021) financed by national funds through the FCT/MCTES (PIDDAC); national funds through FCT/MCTES (PIDDAC): LEPABE, UIDB/00511/2020 (DOI: 10.54499/UIDB/00511/2020) and UIDP/00511/2020 (DOI: 10.54499/UIDP/00511/2020) and ALiCE, LA/P/0045/2020 (DOI: 10.54499/LA/P/0045/2020).

Abstract

The most widely deposition technology used for producing inverted perovskite solar cells (PSCs) is spin-coating, but it has limitations when used on large substrates. The slot-die coating is a promising alternative for deposition on larger areas. This study aimed to optimize the PTAA and perovskite layers deposition using a slot-die coater, considering in its structure a perovskite material stable under ambient air. The device architecture then employed in this study was PTAA/$MAPbI_3$/PCBM/BCP/Ag, chosen for its stability in ambient air. Achieving uniform, thin, and defect-free layers is critical for the proper functioning of inverted PSCs. SEM characterization was employed to evaluate the film quality. Optimization was carried out using the JMP software. The optimized conditions for PTAA layer deposition were: 20 $mm \cdot s^{-1}$ of coating speed, 50 µm gap between the slot-die head and the substrate, 70 ºC plate temperature, a sintering temperature of 100 ºC and a concentration of PTAA solution of 2 $mg \cdot mL^{-1}$. For the perovskite layer, optimal conditions were: 8 $mm \cdot s^{-1}$ coating speed, 65 µm gap between the slot-die head and the substrate, 70 ºC plate temperature, a sintering temperature of 80 ºC and a perovskite concentration of 1.1 $mol \cdot L^{-1}$. Following optimization, the best performing 5 cm^2 device assembled via slot-die coating achieved a power conversion efficiency of 7.32 %, V_{OC} of 0.85 V, J_{SC} of 18.88 $mA \cdot cm^{-2}$ and *FF* of 0.46.

Keywords: Slot-die coating, coating parameters optimization, $MAPbI_3$, inverted PSCs.

Resumo

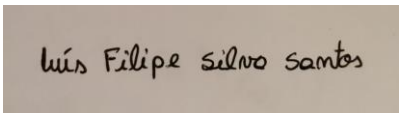
A técnica de *spin-coating* é atualmente a mais usada para a produção de células solares de perovskita invertidas em pequena escala, apresentando limitações para maiores dimensões. Para deposições em áreas maiores uma das tecnologias mais promissoras é *slot-die coating*.

O objetivo principal deste trabalho consistiu na otimização da deposição por *slot-die* da camada transportadora de lacunas, o PTAA, e da camada absorvedora de luz, uma perovskita estável em condições de ar ambiente ($MAPbI_3$). A arquitetura dos dispositivos usados neste estudo foi PTAA/$MAPbI_3$/PCBM/BCP/Ag, escolhida exatamente pela sua estabilidade em ar ambiente. Atingir um filme uniforme, fino e sem defeitos é crucial para um bom funcionamento de uma célula solar de perovskita invertida. A caracterização por SEM foi usada para avaliar a qualidade do filme e a otimização foi feita usando o *software JMP*. As condições otimizadas para a deposição da camada de PTAA foram: 20 $mm \cdot s^{-1}$ para a velocidade de deposição, distância de 50 µm entre a cabeça da *slot-die* e o substrato, 70 ºC para temperatura do prato da *slot-die*, temperatura de sinterização a 100 ºC e uma concentração de PTAA de 2 $mg \cdot mL^{-1}$. Para a camada de perovskita as condições otimizadas foram: 8 $mm \cdot s^{-1}$ para a velocidade do prato da *slot-die*, distância de 65 µm entre a cabeça da *slot-die* e o substrato, 70 ºC para a temperatura do prato, uma temperatura de sinterização de 80 ºC e a concentração de perovskita de 1.1 $mol \cdot L^{-1}$. Utilizando estas condições otimizadas, a célula PSC de 5 cm^2 com melhor desempenho obteve uma eficiência de conversão de energia de 7.32 %, V_{OC} de 0.85 V, J_{SC} de 18.88 $mA \cdot cm^{-2}$ e *FF* de 0.46.

Palavras-chave: *Slot-die coating*, otimização dos parâmetros de deposição, $MAPbI_3$, PSCs invertidas.

Declaration

I hereby declare, under word of honor, that this work is original and that all non-original contributions is indicated and due reference is given to the author and source



Luís Santos, 01/07/2024

Index

1. Introduction 1
1.1. Framing and presentation of the work 1
1.2. Contribution of the author to the work 2
1.3. Organization of the dissertation 3
2. Context and State of the art 5
2.1. Solar cell structure 5
2.2. Inverted perovskite solar cells 6
2.2.1. Glass substrate coated with a TCO 6
2.2.2. Hole transport layer (HTL) 6
2.2.3. Perovskite layer 7
2.2.4. Electron transport layer (ETL) 7
2.2.5. Back contact 8
2.3. Upscaling 8
2.3.1. Spin-coating 9
2.3.2. Slot-die coating 9
2.3.3. Thermal evaporation 11
2.3.4. SEM characterization 12
2.4. *I-V* characterization 12
3. Materials and Methods 17
3.1. Materials 17
3.2. Equipments 17
3.3. Optimized procedure for preparation of inverted PSCs 18
4. Results and discussion 21
4.1. Optimization of PTAA layer 22
4.2. Optimization of perovskite layer 29
5. Conclusion 37
6. Assessment of the work done 39
6.1. Objectives Achieved 39
6.2. Contribution to the Sustainable Development Goals 39
6.3. Final Assessment 40
7. References 41
Annex A - Efficiencies of PSC devices reported in literature according to the active area 45
Annex B - Sustainable Development Goals 47

Appendix A – Set of experiments for PTAA and perovskite layer optimization 49
Appendix B – Principal photovoltaic parameters of solar cells 53
Appendix C – SEM images of the perovskite layer 55

List of Figures

Figure 1.1. Evolution of renewable electricity generation since 2000.[1] 1

Figure 1.2. Annual investment in fossil fuels and clean energy.[2] 1

Figure 1.3. Evolution of the power conversion efficiency of different photovoltaic technologies.[4] ... 2

Figure 2.1. Working mechanism of an inverted PSC. 5

Figure 2.2. Main device architectures of perovskite solar cells: a) regular and b) inverted. 6

Figure 2.3. Crystal structure of $MAPbI_3$ perovskite.[8] 7

Figure 2.4. Evolution of the size of PSC devices and modules fabricated with different deposition methods.[11] 8

Figure 2.5. Schematic process of spin-coating deposition, starting from the dropping of the solution until the evaporation of solvents.[6] 9

Figure 2.6. Scheme of the slot-die coating process. [3] 10

Figure 2.7. Coating window and some typical slot-die coatings defects.[14] 10

Figure 2.8. Schematic representation of the thermal evaporation process.[6] 12

Figure 2.9. Current - potential difference curve for a solar cell. 13

Figure 2.10. Power – potential difference curve for a solar cell. 14

Figure 2.11. Solar cell electrical circuit analogue. 15

Figure 3.1. Equipments used in the preparation of the inverted PSCs: a) a slot-die coater[19], b) a spin-coater[20], c) the thermal evaporator [21], d) the benchtop SEM [22]. 17

Figure 4.1. Structure of the inverted PSC used in this work. 21

Figure 4.2. I-V characterization of the dummy cell delivering lower ohmic resistance of PTAA layer. Deposition conditions: 70 ºC of plate temperature, 20 $mm \cdot s^{-1}$ coating speed, 2.00 $mg \cdot mL^{-1}$ of concentration of PTAA and 50 µm of gap. 23

Figure 4.3. Prediction profile from JMP software for the first optimization of PTAA deposition. 23

Figure 4.4. Prediction profile from JMP software for the second optimization of PTAA deposition. ... 24

Figure 4.5. Top-view images of the surface morphology of the perovskite layer using SEM characterization. 26

Figure 4.6. SEM images of perovskite layer using a sintering temperature of 100 ºC and different slot-die plate temperatures: a) 35 ºC, b) 40 ºC, c) 50 ºC, d) 60 ºC, e) 70 ºC, f) 80 ºC. 27

Figure 4.7. SEM images of the perovskite layer using different sintering temperatures: a) 80 ºC, b) 100 ºC. 27

Figure 4.8. Photovoltaic performance parameters of the PSC devices prepared based on the three selected conditions for the PTAA slot-die deposition: a) V_{OC}, b) J_{SC}, c) FF, d) PCE. 28

Figure 4.9. I-V curve for a complete PSC device. Deposition conditions: 70 ºC for the slot-die plate temperature, 80 ºC for sintering temperature, 10 mm·s^{-1} coating speed, 1.1 mol·L^{-1} of perovskite concentration and 50 µm Gap. 29

Figure 4.10. Prediction profile from JMP software for the perovskite optimization. 30

Figure 4.11. Photovoltaic performance parameters of the PSC devices prepared with the optimal conditions obtained with optimized perovskite slot-die deposition: a) V_{OC}, b) J_{SC}, c) FF, d) PCE. 32

Figure 4.12: SEM images of PSC device prepared with optimized slot-die coating conditions: a) top-view, and b) cross-section. 33

Figure 4.13. PSC device divided into 3 small cells to evaluate the quality of the slot-die coating deposition. 33

Figure 4.14. Current Density - potential difference curve for a full PSC device (5 cm^2) and its segmented parts (2.2 cm^2). 34

Figure 4.15. PCE of PSC devices prepared using slot-die coating (at least the perovskite layer) as a function of the active area. Individual solar cells are represented by circles and modules are represented by squares. The blue color refers to devices produced under ambient air and the green color to devices made in a controlled atmosphere. The best-performing PSC device obtained based on this work is represented with a triangle. Adapted from ref. [25]. 35

Figure An. B. 1. Sustainable Development Goals.[40] 47

Figure Ap. C. 1. SEM images: a) top-view, and b) cross-section (perovskite slot-die deposition conditions: 8 mm·s^{-1} coating speed, 0.75 mol·L^{-1} of perovskite solution concentration and 50 µm of gap). 55

Figure Ap. C. 2. SEM images: a) top-view, and b) cross-section (perovskite slot-die deposition conditions: 10 mm·s^{-1} coating speed, 0.75 mol·L^{-1} of perovskite solution concentration and 50 µm of gap). 55

Figure Ap. C. 3. SEM images: a) top-view, and b) cross-section (perovskite slot-die deposition conditions: 25 mm·s^{-1} coating speed, 0.75 mol·L^{-1} of perovskite solution concentration and 50 µm of gap). 56

Figure Ap. C. 4. SEM images: a) top-view, and b) cross-section (perovskite slot-die deposition conditions: 8 mm·s^{-1} coating speed, 0.75 mol·L^{-1} of perovskite solution concentration and 125 µm of gap). 56

Figure Ap. C. 5. SEM images: a) top-view, and b) cross-section (perovskite slot-die deposition conditions: 16.5 mm·s^{-1} coating speed, 0.75 mol·L^{-1} of perovskite solution concentration and 125 µm of gap). 57

Figure Ap. C. 6. SEM images: a) top-view, and b) cross-section (perovskite slot-die deposition conditions: 25 mm·s^{-1} coating speed, 0.75 mol·L^{-1} of perovskite solution concentration and 125 µm of gap). *57*

Figure Ap. C. 7. SEM images: a) top-view, and b) cross-section (perovskite slot-die deposition conditions: 16.5 mm·s^{-1} coating speed, 1.00 mol·L^{-1} of perovskite solution concentration and 50 µm of gap). *58*

Figure Ap. C. 8. SEM images: a) top-view, and b) cross-section (perovskite slot-die deposition conditions: 25 mm·s^{-1} coating speed, 1.00 mol·L^{-1} of perovskite solution concentration and 50 µm of gap). *58*

Figure Ap. C. 9. SEM images: a) top-view, and b) cross-section (perovskite slot-die deposition conditions: 8 mm·s^{-1} coating speed, 1.00 mol·L^{-1} of perovskite solution concentration and 125 µm of gap). *59*

Figure Ap. C. 10. SEM images: a) top-view, and b) cross-section (perovskite slot-die deposition conditions: 16.5 mm·s^{-1} coating speed, 1.00 mol·L^{-1} of perovskite solution concentration and 125 µm of gap). *59*

Figure Ap. C. 11. SEM images: a) top-view, and b) cross-section (perovskite slot-die deposition conditions: 8 mm·s^{-1} coating speed, 1.25 mol·L^{-1} of perovskite solution concentration and 50 µm of gap). *60*

Figure Ap. C. 12. SEM images: a) top-view, and b) cross-section (perovskite slot-die deposition conditions: 10 mm·s^{-1} coating speed, 1.25 mol·L^{-1} of perovskite solution concentration and 50 µm of gap). *60*

Figure Ap. C. 13. SEM images: a) top-view, and b) cross-section (perovskite slot-die deposition conditions: 25 mm·s^{-1} coating speed, 1.25 mol·L^{-1} of perovskite solution concentration and 50 µm of gap). *61*

Figure Ap. C. 14. SEM images: a) top-view, and b) cross-section (perovskite slot-die deposition conditions: 8 mm·s^{-1} coating speed, 1.25 mol·L^{-1} of perovskite solution concentration and 125 µm of gap). *61*

Figure Ap. C. 15. SEM images: a) top-view, and b) cross-section (perovskite slot-die deposition conditions: 16.5 mm·s^{-1} coating speed, 1.25 mol·L^{-1} of perovskite solution concentration and 125 µm of gap). *62*

List of Tables

Table 2.1. Large-area inverted PSCs prepared using slot-die coating. 11

Table 4.1. Process values and their corresponding limits for the first optimization of PTAA. 22

Table 4.2. Process values and their corresponding limits for the second optimization of PTAA. 24

Table 4.3. Range of temperatures studied..... 26

Table 4.4. Conditions of PTAA used for preparing full PSC devices. 28

Table 4.5. Process values and their corresponding ranges for the perovskite slot-die deposition optimization. 30

Table 4.6. Relationship between the coating conditions used and defects observed. 31

Table An. A 1. PSC devices produced in ambient air conditions. 45

Table An. A 2. PSC devices produced in a controlled atmosphere. 46

Table Ap. A. 1. Set of experiments to be performed according to JMP software and the results obtained for the first PTAA optimization. 49

Table Ap. A. 2. Set of experiments to be performed according to JMP software and the results obtained for the second PTAA optimization. 50

Table Ap. A. 3. Set of experiments to be performed according to JMP software and the results obtained for the perovskite optimization..... 51

Table Ap. B. 1. Principal photovoltaic parameters of full PSCs prepared with the selected deposition conditions of PTAA, under illumination of 1 sun (100 mW·cm^{-2}, AM 1.5, room temperature). 53

Table Ap. B. 2. Principal photovoltaic parameters of full PSCs prepared with the optimized deposition conditions of perovskite layer, under illumination of 1 sun (100 mW·cm^{-2}, AM 1.5, room temperature). 53

Table Ap. B. 3. Principal photovoltaic parameters of full PSC devices and the segmented device prepared using the optimized PTAA and perovskite slot-die conditions. 54

Notation and Glossary

List of variables

A	Active area	cm^2
Ca	Capillary number	-
D	Diode	-
H_0	Gap	μm
I	Electric current	mA
J	Current density	$mA \cdot cm^{-2}$
n	Ideality factor	-
P	Power	$W \cdot cm^{-2}$
Q	Pumping rate	$L \cdot s^{-1}$
R	Resistance	Ω
t	Thickness	μm
T	Temperature	$^{\circ}C$
U	Coating speed	$mm \cdot s^{-1}$
V	Potential difference	V
w	Width coating	mm

List of constants

k	Boltzmann constant (1.380649×10^{-23} $m^2 \cdot kg \cdot s^{-2} \cdot K^{-1}$)
q	Elementary Charge ($1.60217663 \times 10^{-19}$ C)

Indexes

D	Diode
inc	Incident
max	Maximum
OC	Open circuit
S	Series
SC	Short-circuit
SH	Shunt
wet	Wet film
0	Dark Saturation

List of Acronyms

BCP	2,9-dimethyl-4,7-diphenyl-1,10-phenanthroline
ETL	Electron transport layer
FF	Fill Factor
FTO	Fluorine-doped tin oxide
HOMO	Highest occupied molecular orbitals
HTL	Hole transport layer

ITO	Indium tin oxide
MA	Methylammonium
MAI	Methylammonium iodide
$MAPbI_3$	Methylammonium lead triiodide
PbI_2	Lead iodide
PCBM	[6,6]-Phenyl-C61-butyric acid methyl ester
PCE	Power Conversion Efficiency
PTAA	Poly[bis(4-phenyl)(2,4,6-trimethylphenyl)amine
PSC	Perovskite solar cell
SEM	Scanning Electron Microscopy
TCO	Transparent conductive oxide

1. Introduction

1.1. Framing and presentation of the work

Nowadays, both population and economic growth are accelerating. Indeed, the demand for electricity is anticipated to rise significantly to accommodate the needs of an expanding populace. Given the finite nature of fossil fuels, it is imperative to explore alternative and efficient methods of energy production. Embracing renewable energy sources not only promises to meet our increasing energy demands, but also offers a sustainable path to diminish our reliance on depleting fossil fuels. Figure 1.1 shows the evolution of renewable electricity generation since 2000 and it is expected that more than 40 % of electricity will be generated from renewable energy sources by 2028. Over the past decade, solar and wind technologies have seen the most significant advancements. Presently, their combined energy production rivals that of hydropower. This remarkable growth has been driven by heightened investment in clean energy generation, as illustrated in Figure 1.2.

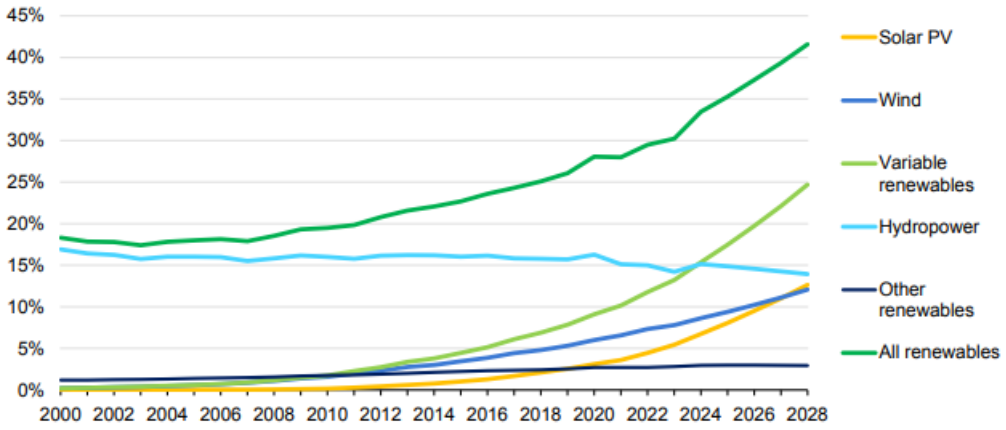


Figure 1.1. Evolution of renewable electricity generation since 2000.[1]

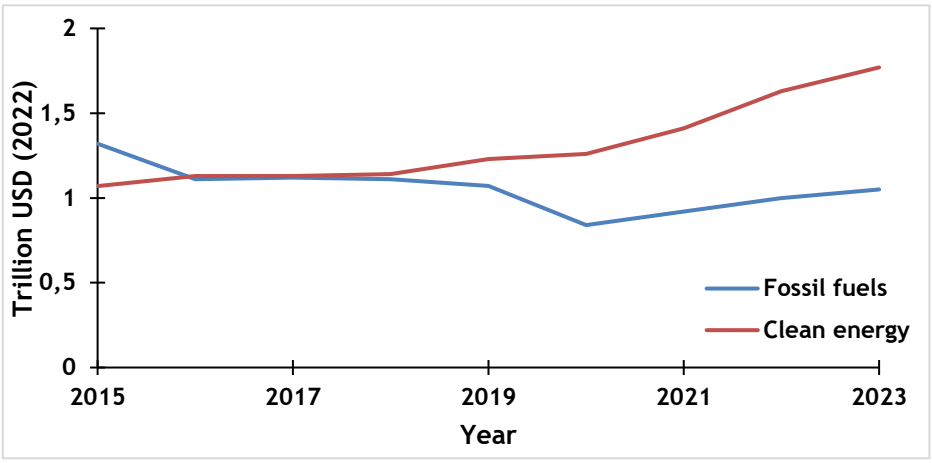


Figure 1.2. Annual investment in fossil fuels and clean energy.[2]

This study will focus on solar energy, specifically addressing solar cell technology, which converts solar energy into electrical energy. Within the field of photovoltaics, organic-inorganic perovskite solar cells (PSCs) are gaining much attention due to their compatibility with flexible materials, cost-effective manufacturing, solution-processability, and highly tunable band gaps, making them highly efficient to be commercially competitive.[3] Figure 1.3 illustrates the efficiency evolution of perovskite solar cells, with their power conversion efficiency (*PCE*) rising from 13.8 % in 2013 to 26.1 % in 2024, indicating their potential to rival conventional solar cells.[4]

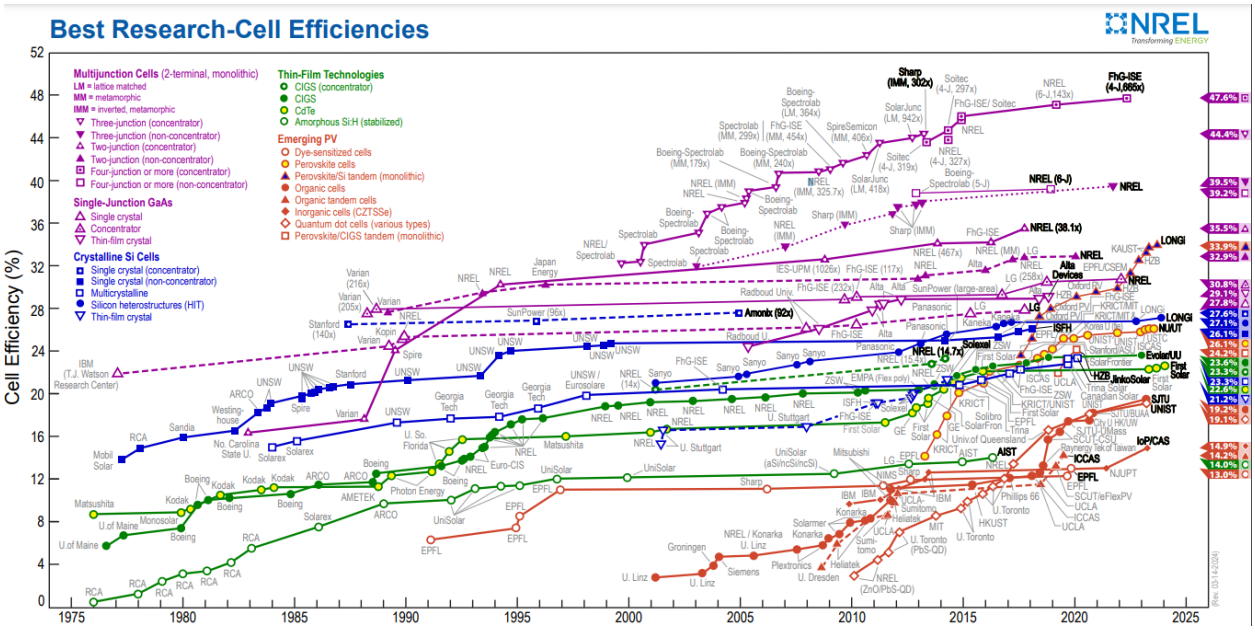


Figure 1.3. Evolution of the power conversion efficiency of different photovoltaic technologies.[4]

This work focuses on the successful deposition of HTL (PTAA) and perovskite layers, under ambient air conditions using slot-die coating technology. The use of this technology allows the scalability of the devices. The coating optimization of these two layers was carried out using the software JMP 18.0.1.

1.2. Contribution of the author to the work

All the experimental work was carried out by the author based on procedures already implemented in the host laboratory. In particular, all the solutions and respective calculations were performed by the author, as well as all the depositions by slot-die and spin-coating. The Design of Experiments using the software JMP, as well as the characterization based on photovoltaic performance were also independently performed by the author. Finally, the experimental data was treated and interpreted by the author, and the main conclusions were discussed with the supervisors.

1.3. Organization of the dissertation

This work is divided into six parts. Firstly, in Chapter 1, the project is described and the objectives are briefly explained. The second chapter presents the perovskite solar cells technology, the functions of different layers, the most important technologies used in their deposition, and a theoretical interpretation of the photovoltaic parameters used to characterize cell performance. The third chapter describes the materials and experimental procedure used to develop the proposed experimental work. The fourth chapter presents the results and discussion. The fifth chapter contains the conclusions of this work. Finally, the last chapter presents the main objectives achieved and the contribution of this project to the sustainable development goals.

2. Context and State of the art

2.1. Solar cell structure

A solar cell is an electronic device that converts sunlight into electricity. As depicted in Figure 2.1, this process requires a material such as a perovskite that, upon absorbing sunlight, excites electrons to a higher energy state. When the incident energy exceeds the band gap, electron-hole pairs are created. The excited electrons move to the electron transport layer (ETL), while holes move to the hole transport layer (HTL). Electrons travel through the external circuit, generating power, before returning to the solar cell and recombining with holes in the p-type layer. If recombination occurs prematurely within the cell, the electron-hole pair is lost, resulting in no electric current in the external circuit and no power generation.

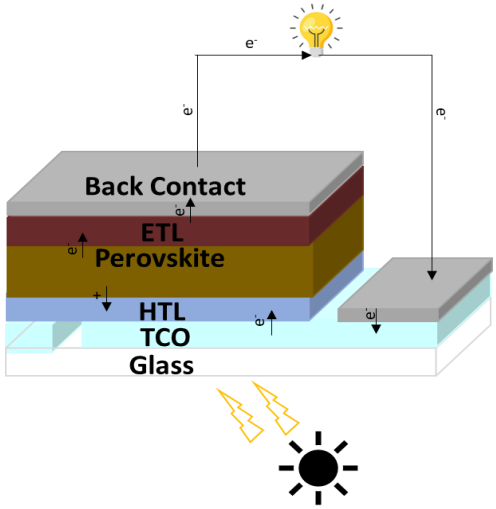


Figure 2.1. Working mechanism of an inverted PSC.

The photovoltaic performance success of PSCs is due to the excellent optical and electrical properties of the perovskite structure family used for these applications, such as the tunable band gap, the large optical absorption coefficient and the high carrier mobility. The high light absorption coefficient enables the use of a very thin perovskite absorber layer to collect the light, resulting in a reduced charge carrier transport length and material consumption.[5] Throughout the development of PSC devices, various device structures have been reported. The most common structures are the regular (both planar and mesoporous) and the inverted configurations, as illustrated in Figure 2.2. In this work, the focus will be on the inverted perovskite solar cells.

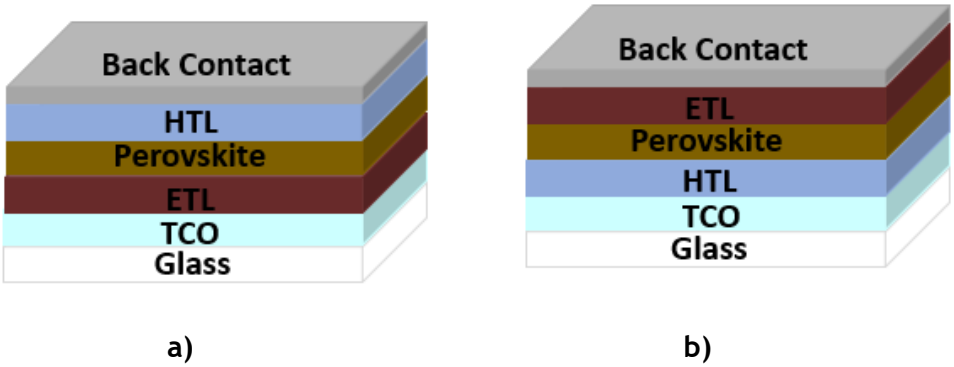


Figure 2.2. Main device architectures of perovskite solar cells: a) regular and b) inverted.

2.2. Inverted perovskite solar cells

The inverted architecture, as opposed to the regular configuration, has the HTL deposited on top of the transparent conductive oxide (TCO) material and the ETL deposited after the perovskite layer, which influences the direction of charge carrier extraction and the materials used for each layer. This configuration can offer advantages in stability and manufacturing, contributing to its growing popularity in photovoltaic research and applications. Indeed, inverted PSCs often exhibit better stability, especially under environmental stress conditions such as humidity and temperature. This is partly because the materials used in the inverted architecture can be more resistant to degradation. Then, inverted configurations typically show less hysteresis in their current- potential difference characteristics, leading to more accurate and consistent measurements of their performance. Finally, the fabrication process for inverted PSCs can be simpler and more compatible with existing industrial processes, especially those used for flexible substrates and roll-to-roll manufacturing processes.

2.2.1. Glass substrate coated with a TCO

As glass is not a conductive material, it must be coated with a transparent conducting oxide which enables the glass substrate conductivity. Two types of TCO are used to prepare perovskite solar cells, fluorine-doped tin oxide (FTO) and indium tin oxide (ITO). FTO was the glass substrate selected for this work.

2.2.2. Hole transport layer (HTL)

The hole transport layer is positioned on top of the FTO substrate. This layer selectively extracts and transports holes, being a p-type semiconductor material, which is a material with a deficit of electrons. This layer must satisfy the following requirements: 1) the highest occupied molecular orbital, HOMO, or the valence band of the HTL must be compatible with the perovskite film, -5.4 eV; 2) it must have a high hole mobility; 3) since this layer is between the

glass and the perovskite, the HTL must have a high optical transmittance within the absorption range of the perovskite (300-800 nm) to avoid photon loss; 4) HTL must not react with the perovskite to avoid its decomposition; 5) it must be stable under ambient conditions and solution processable.[6] Within this work, PTAA was used as HTL.

2.2.3. Perovskite layer

Perovskites are a family of materials with a crystalline structure ABX_3, where A and B are cations of different sizes, and X is an anion. $MAPbI_3$, the perovskite normally used under air conditions and used in this work, has a large cation A, methylammonium ($CH_3NH_3^+$, MA^+), a smaller cation B, lead (Pb^{2+}) and the X, a halogen ion, iodine (I^-) [7]. Its crystal structure can be described as $[PbI_6]^{4-}$ octahedra connected in space with corner-sharing vertices to form a three-dimensional structure, and MA^+ cations filling the pores to create an electrically neutral environment, as shown in Figure 2.3.

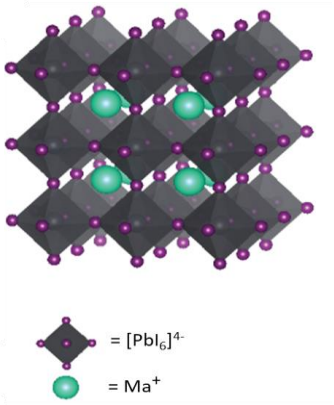


Figure 2.3. Crystal structure of $MAPbI_3$ perovskite.[8]

$MAPbI_3$ has a tunable band gap, a high light absorption coefficient, noticeable photovoltaic properties, high power conversion efficiencies (*PCE* = 14–20 %), low exciton binding energy, and long carrier diffusion length. As a result, the perovskite absorbing layer can be thinner, which is beneficial to reduce the transport length of the charges, the material usage and recombination between pair electron-hole. This perovskite also has some advantages like long-term stability, easy crystallization at low temperatures, and simple fabrication.[5, 9]

2.2.4. Electron transport layer (ETL)

The electron transport layer is deposited on top of the perovskite layer. The ETL is important for transporting electrons, being an n-type semiconductor material, which is a material with an excess of electrons. Some aspects must be considered when choosing the ETL to be used: 1) it must have high electron mobility and efficient hole-blocking properties; 2) the deposition process for this layer must be compatible with the perovskite layer to minimize defects in it;

3) this layer must completely cover the perovskite layer as if there is contact between the perovskite and the back contact, it can lead to rapid degradation of the perovskite; 4) there must be no reactions between these layers.[6] The ETL used for this work was PCBM.

2.2.5. Back contact

The materials used in this layer are essentially conductive metals, being the most used silver and gold, due to their excellent electrical conductivity. As previously mentioned, the perovskite layer can suffer corrosion or contamination when in contact with the back contact, turning the silver back contact slightly yellow a few days after its manufacture as a result of the silver oxidation to silver iodide. It is important for this layer to be stable under ambient conditions and to minimize ion diffusion-induced device degradation to increase the stability of the cell.[6]

2.3. Upscaling

Upscaling is particularly challenging in solution-processed films, where precise control of film uniformity is needed to avoid material defects. Over the years, several deposition methods have been reported for the deposition of PSC layers such as HTL, perovskite and ETL layers over large areas, while back contact is normally deposited by thermal evaporation.[10] For laboratory-scale devices, spin-coating is the most efficient deposition method, but as the scale increases, it becomes more difficult to crystallize and form a uniform perovskite film. Currently, one of the most promising methods for perovskite deposition over large areas is slot-die coating - Figure 2.4.

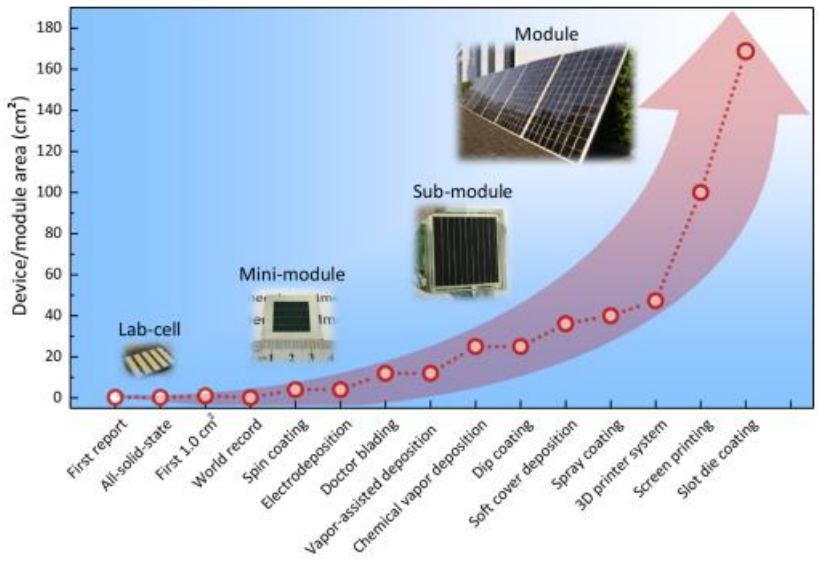


Figure 2.4. Evolution of the size of PSC devices and modules fabricated with different deposition methods.[11]

2.3.1. Spin-coating

Spin-coating is the most used technique to deposit uniform thin films on flat and small substrates. The spin-coating technique just needs a small amount of coating material solution, which is applied on the center of the substrate while the substrate is spinning at low speed or not spinning at all. Then the substrate is rotated at high angular speed to spread the coating material by centrifugal force. The spin-coated film will be treated under thermal treatment to evaporate the solvents, as represented in Figure 2.5.[6] However, this deposition technique is not recommended for large substrates, since it is difficult to ensure uniform and high-quality films over large areas. Moreover, there is a lot of wasted solution and, if the substrate is flexible or has any roughness, it makes this process more difficult to form a thin film.

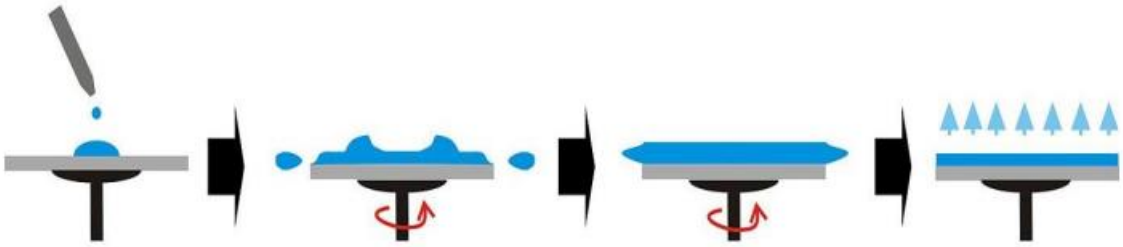


Figure 2.5. Schematic process of spin-coating deposition, starting from the dropping of the solution until the evaporation of solvents.[6]

2.3.2. Slot-die coating

Slot-die coating, exemplified in Figure 2.6, is a versatile deposition process widely used for producing thin and uniform films, and it is the most promising deposition technology for upscaling PSCs since it can also be used with flexible substrates. This process involves the delivering of a solution to a moving substrate through a narrow slit in the slot-die head. A meniscus is formed when the solution contacts with the substrate, and the film extends along the coating direction. When the ink solution delivery is not made using a syringe pumping, but by manually dispensing a certain volume of ink solution on the substrate, a blade coating deposition process occurs.

Achieving thin and uniform layers through slot-die deposition requires careful optimization of several key parameters. These include the gap between the slot-die head and the substrate, the plate speed and the temperature, and the flow/volume of the solution. Variation in these parameters during slot-die coating can lead to coating defects, such as rivulets, ribbing, air entrainment, and swelling and weeping at the upstream meniscus (Figure 2.7). These defects

can affect the quality and consistency of the coated layers, highlighting the importance of precise control and optimization in the manufacturing process. Rivulets are alternating coated and uncoated stripes in the coating direction and they occur when the pressure difference between the upstream and downstream meniscus is too high. Ribbing is a thickness undulation on the deposited layer caused by excessive viscous forces that exceed the capillary force of the meniscus. Air entrainment occurs when air bubbles become trapped within the coated film caused due to high maximum wetting velocities. Swelling and weeping at the upstream meniscus is caused by the decrease in the coating speed and the upstream meniscus is pulled out past the slot-die head.[12, 13]

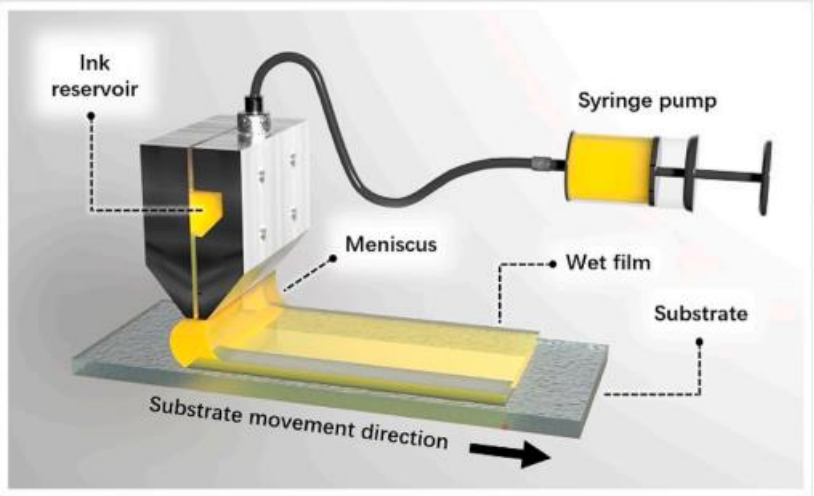


Figure 2.6. Scheme of the slot-die coating process. [3]

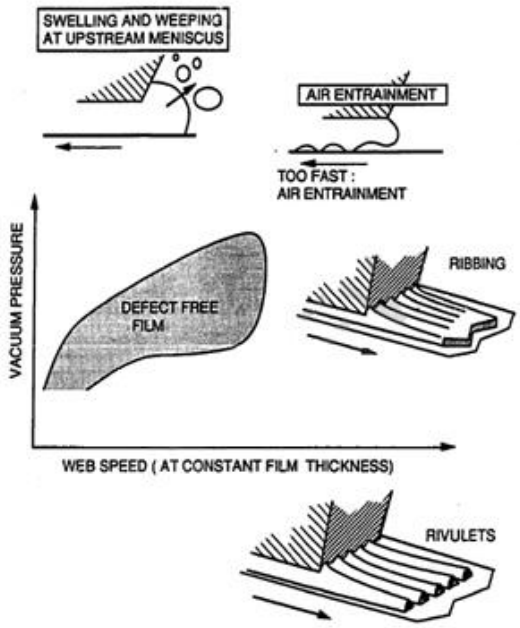


Figure 2.7. Coating window and some typical slot-die coatings defects.[14]

Table 2.1 shows some literature examples of large area inverted PSCs in which at least one layer was deposited by slot-die coating.

Table 2.1. Large-area inverted PSCs prepared using slot-die coating.

Device structure	Slot-die coated layer	Area (cm^2)	PCE (%)	Year/Ref.
ITO/PEDOT:PSS/$MAPbI_{3-x}Cl_x$/PCBM/BCP/Ag	Perovskite	8.30	10.0	2018/[15]
FTO/NiO/$MAPbI_3$/G-PCBM/BCP/Ag	Perovskite	36.10	15.6	2019/[16]
FTO/NiO_x/$MAPbI_3$/PCBM/PEI/Ag	Perovskite	3.78	10.3	2020/[10]
ITO/PTAA/$MAPbI_3$/C_{60}/BCP/Cu	HTL, Perovskite	6.80	14.4	2020/[17]

2.3.3. Thermal evaporation

Thermal evaporation is a widely used technique for depositing thin films. It is particularly suited for materials like metal electrodes that require precise thickness control or are challenging to deposit using solution-based methods. In this process, the precursor material evaporates under vacuum conditions as soon as it reaches its boiling point, facilitating rapid evaporation and deposition onto substrates, as shown in Figure 2.8. For perovskite solar cell devices, thermal evaporation is predominantly used for depositing metal electrodes onto the surface of the ETL. This method enables the formation of uniform and dense electrodes with a controllable deposition rate and total thickness. [6]

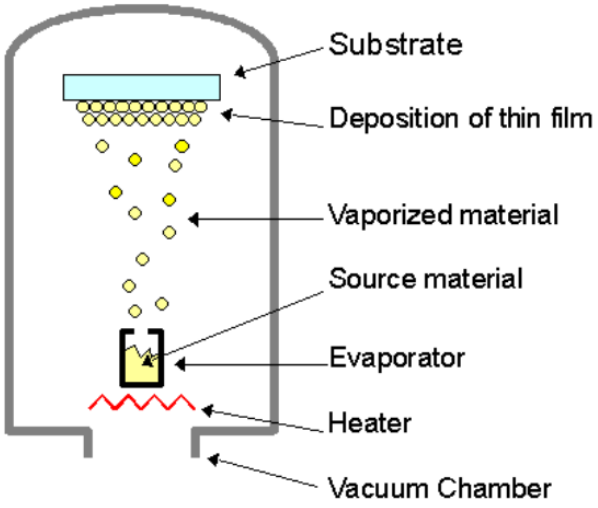


Figure 2.8. Schematic representation of the thermal evaporation process.[6]

2.3.4. SEM characterization

Scanning Electron Microscopy (SEM) is a type of electron microscope that uses a focused electron beam to scan sample surfaces to produce images. The electrons in the beam could interact with the atoms inside the sample, producing a variety of signals that can be used for collecting information about the samples including surface morphology, topography, and composition. SEM can also be used to examine the surface morphology including roughness, surface coverage and thickness of a film when a cross-sectional analysis is performed.[6]

2.4. *I-V* characterization

The principal photovoltaic parameters for the analysis of the performance of a solar cell are the short-circuit current (I_{SC}), the open-circuit potential difference (V_{OC}), the maximum power (P_{max}), the fill factor (FF) and Power Conversion efficiency (PCE). These parameters can be obtained by mean of the corresponding current-potential difference (*I-V*) curves - Figure 2.9.

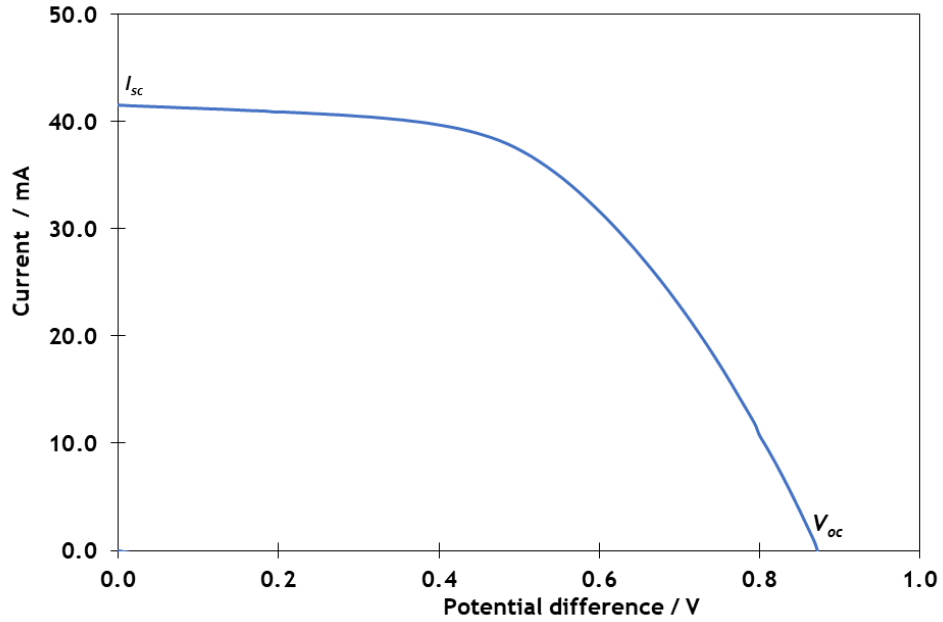


Figure 2.9. Current - potential difference curve for a solar cell.

The *I-V* curve can be described by the following equation:

$$I = I_{\text{inc}} - I_0 \times e^{\frac{qV}{nkT}} \tag{2.1}$$

where I_{inc} is the light-generated electric current, that is produced in the presence of sunlight, and $I_0 \times e^{\frac{qV}{nkT}}$ is the diode equation, which represents the current flowing through the diode I_D, where I_0 is the "dark saturation current". Actually, the p-n junction in all photovoltaic devices behaves as a diode, so, the *I-V* curve of a solar cell is the superposition of the *I-V* curve of a diode in the dark with the light-generated current. The dark saturation current I_0 is proportional to temperature and decreases with enhanced material quality; q is the elementary charge; *V* is the applied potential difference across the terminals of the diode, *n* is the ideality factor (a number between 1 and 2, which increases as the current decreases); *k* is the Boltzmann constant; and *T* is the absolute temperature. Equation 2.1 relates the electric current with the potential difference, but as the diode equation increases exponentially with increasing potential difference, this leads to an exponential decrease in the current flowing through the external circuit.[18]

Looking together at Figure 2.9 and Figure 2.10, when there is no applied potential difference all electrons photogenerated circulate through the external circuit but no power is produced by the solar cell. This is the short-circuit situation. When the potential difference is disturbed, there is a decrease in the electric field at the p-i-n junction and, according to the diode equation, more electrons are needed to balance the junction, and reach equilibrium again. The remaining electrons perform work in the external circuit, and they are accounted by the

electrochemical station, producing the corresponding power. However, when the limit situation is reached in which all the light-generated electrons are needed to balance the p-i-n junction and no electrons circulate in the external circuit, no power is generated by the solar cell. This is the open circuit situation. So, returning to Figure 2.9, one can see that there are two characteristic points on this curve: i) a short-circuit situation corresponding to zero potential difference and maximum current (I_{SC}) and ii) an open-circuit situation in which the potential difference is maximum, and the current is zero (V_{OC}). In both cases, no power is produced, so these points are not relevant for an operating solar cell.[18] Indeed, the point of interest in operating any solar cell is when the maximum power (P_{max}) is achieved, meaning that, simultaneously, maximum current and maximum potential difference are reached - Figure 2.10.

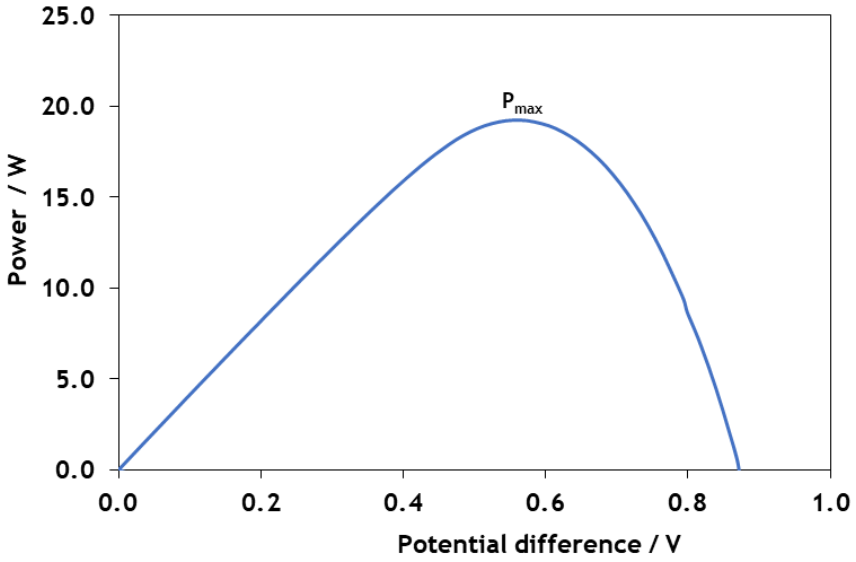


Figure 2.10. Power - potential difference curve for a solar cell.

Another relevant performance parameter is the fill factor (FF), which is the ratio between the maximum power obtained from a solar cell and the product of V_{OC} and I_{SC} - Equation 2.4. This value varies between 0 and 1, and higher values mean more efficient devices.

To calculate the PCE, given the maximum power of the cell and knowing the incident power (100 mW·cm^{-2} for 1 simulated sun), the efficiency is calculated using Equation 2.5.

$$V = R \times I \tag{2.2}$$

$$P = V \times I \tag{2.3}$$

$$\mathrm{FF} = \frac{P_{max}}{I_{SC} \times V_{OC}} \tag{2.4}$$

$$\text{PCE}\ (\%) = \frac{P_{max}}{P_{inc}} \times 100 \tag{2.5}$$

Important to mention that some power dissipation may occur for an operating solar cell due to resistive effects. The most common resistances are series resistance, R_S, and shunt resistance, R_{SH}, illustrated in Figure 2.11. Series resistance in a solar cell may arise from the contact resistance between the metal contacts and the absorber, and the resistance in the front and back metal contacts. This resistance primarily decreases the fill factor, but if it becomes too high, it can also lower the short-circuit current. On the other hand, significant power losses due to shunt resistance (R_{SH}) are generally attributed to manufacturing defects rather than poor solar cell design. Low shunt resistance causes power losses by creating an alternate pathway for the light-generated current, which reduces the current flowing through the solar cell and lowers the cell's potential difference. [18]

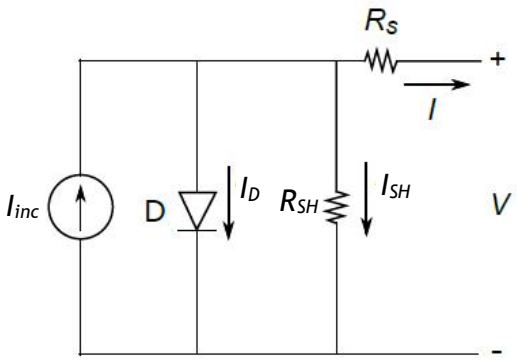


Figure 2.11. Solar cell electrical circuit analogue.

In the presence of both series and shunt resistances, the *I-V* curve of the solar cell can now be written as follows in Equation 2.6:

$$I = I_{inc} - I_D - I_{SH} = I_{inc} - I_0 \times e^{\frac{q(V+I R_S)}{nkT}} - \frac{V+IR_S}{R_{SH}} \tag{2.6}$$

3. Materials and Methods

3.1. Materials

The FTO-coated glass substrates (7 $\Omega \cdot sq^{-1}$) were purchased from Greatcell Solar Materials. Poly[bis(4-phenyl)(2,4,6-trimethylphenyl)amine] (PTAA) and [6,6]-Phenyl-C_{61}-butyric acid methyl ester (PCBM) were purchased from Ossila. Bathocuproine (BCP, 99.99 % purity) was purchased from Sigma-Aldrich. Perovskite films were fabricated using lead iodide (PbI_2, 99.99 % purity) purchased from TCI and methylammonium iodide (MAI, ≥99 % purity) purchased from Sigma-Aldrich. Acetonitrite (ACN, anhydrous 99.8 % purity) was purchased from Sigma-Aldrich and methylamine (MA(MeOH), 40 % in methanol) was purchased from TCI. Anhydrous toluene was purchased from Carlo Erba Reagents S.A.S. Acetone and anhydrous 2-propanol (IPA) were purchased from Sigma-Aldrich. Silver (Ag, 99.999 % purity) pellets were purchased from Photon Export.

3.2. Equipments

The following equipment was used to prepare inverted PSCs in this work: a slot-die coater [19] - Figure 3.1a, a spin-coater (SPS-Europe, POLOS) - Figure 3.1b, and a thermal evaporator (Oxford Vacuum Science) - Figure 3.1c. To analyze the morphology of the films a scanning electron microscope (SEM, Desktop Phenom XL) was used - Figure 3.1d.

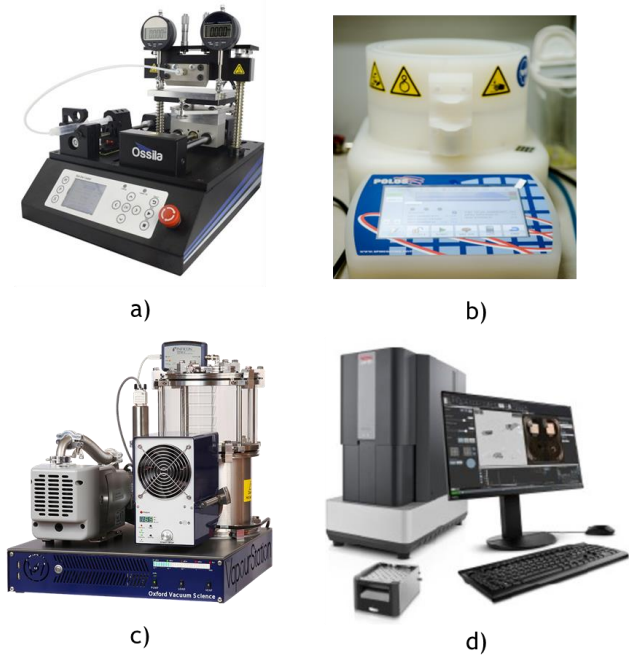


Figure 3.1. Equipments used in the preparation of the inverted PSCs: a) a slot-die coater[19], b) a spin-coater[20], c) the thermal evaporator [21], d) the benchtop SEM [22].

3.3. Optimized procedure for preparation of inverted PSCs

The $MAPbI_3$-based PSCs are fabricated using the inverted p-i-n architecture (FTO/PTAA/$MAPbI_3$/PCBM/BCP/Ag) and under ambient air, except for the PCBM and BCP layers that were deposited in a glovebox filled with N_2.

The FTO glass substrates were scribed using a laser ablation system (a 355 nm UV laser source of 5 W power with a pulse frequency range of 20-200 kHz and a minimum pulse width of 15 ns) to cut the FTO layer. The substrates were then cleaned with a 10 % aqueous solution of Hellmanex and distilled water. Then, the substrates were cleaned with distilled water under ultra-sonication for 10 min, followed by acetone and isopropanol for 15 min each. Then, the substrates were dried with a N_2 stream and subjected to air plasma treatment for 15 min. The cleaned FTO samples were then coated with a thin layer of PTAA as a hole transport layer. The substrate was placed at the slot-die plate at 70 ^{o}C for 5 min. Then, 200 µL of 2 mg·mL^{-1} of PTAA dissolved in toluene was dispensed onto the substrate to form the meniscus. The coating speed and the gap between the substrate and the slot-die head were set at 20 mm·s^{-1} and 50 µm. After PTAA deposition, the substrate was annealed at 100 ^{o}C for 10 min.

For $MAPbI_3$ film, a 1.1 mol·L^{-1} solution of PbI_2 and MAI dissolved in ACN:MA(MeOH) with a volume ratio of 6:4 was prepared. The temperature of the slot-die plate was kept at 70 ^{o}C during the coating process, and to ensure that the substrate was at the coating temperature, FTO/PTAA substrates were placed in the plate for 5 min before starting the deposition. Then, 175 µL of $MAPbI_3$ solution was dispensed into the substrate, and the slot-die deposition was performed with a coating speed and gap set at 8 mm·s^{-1} and 65 µm, respectively. The slot-die coated $MAPbI_3$ samples were subjected to annealing at 80 ^{o}C for 10 min.

On top of the perovskite film, it was dropped 200 µL of 20 mg·mL^{-1} of PCBM dissolved in chlorobenzene; the sample was spun with a spin-coater (4000 rpm during 40 s) and then, annealed at 100 ^{o}C for 10 min. After cooling down at room temperature, 250 µL of 0.5 mg·mL^{-1} of BCP dissolved in 2-propanol was spun in the spin-coater (4000 rpm for 30 s). Finally, 80 nm of Ag (back contact) was deposited by thermal evaporation under vacuum.[23]

The complete devices were characterized right after their preparation under air ambient and temperature conditions. A black mask with 5 cm^2 was used to define the active area.

A solar simulator (150 W Oriel class A) calibrated using a silicon photodiode crystal (Newport, USA) was used to simulate the power corresponding to 1 sun (100 mW·cm^{-2}). The *I-V* curve was obtained by applying an external potential difference using a Zennium electrochemical station (Zahner Elektrik, Germany) and measuring the generated current using Thales software (Thales XT 5.1.4). The scan speed and potential difference step used were 20 mV·s^{-1} and 10 mV, respectively.

The optimization procedure is necessary to obtain the best slot-die operating conditions. To do the optimization, response surface methodology was used and implemented in a commercial software (JMP). This method effectively minimizes the experimental effort by combining mathematical and statistical tools for the investigation of processes in which the responses depend on several variables.

4. Results and discussion

The architecture of the inverted PSCs reported in this work is presented in Figure 4.1, comprising FTO/PTAA/$MAPbI_3$/PCBM/BCP/Ag.

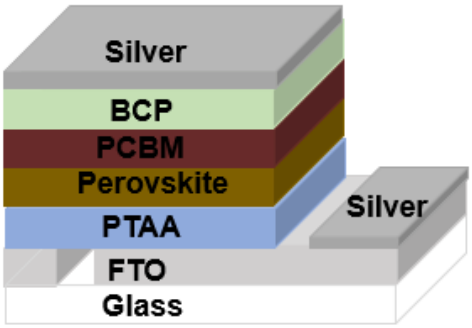


Figure 4.1. Structure of the inverted PSC used in this work.

This work is divided into two parts: the optimization of the HTL layer deposition and the optimization of perovskite layer deposition both using slot-die coating. To optimize the deposition of the active layers on the slot-die coater, the influence of several parameters was first studied, including the gap between slot-die head and substrate, the coating speed, the concentration of the precursor solution, and the temperature of the slot-die plate. The viscocapillary model of slot-die coating can be used to identify the optimal ranges of operating parameters and to explain the impact of each operating parameter on the film quality.[24] The capillary number (*Ca*) is a dimensionless number that represents the ratio between the viscous and surface tension forces of a specific solution, according to equation 4.1:

$$Ca = 0.65\left(\frac{2}{\frac{H_0}{t_{wet}} - 1}\right)^{\frac{3}{2}} \tag{4.1}$$

$$t_{wet} = \frac{Q}{w \cdot U} \tag{4.2}$$

where H_0 is the gap between the slot-die head and substrate, t_{wet} is the wet film thickness, Q is the pumping rate, w is the coating width and U is the coating speed. Using Equation 4.1 and recognizing that the capillary number depends on the solution used, the variables influencing the equation are the ratio between the gap, H_0, and the wet film thickness, t_{wet}. Since the volume of the solution, Q, and the coating width, w, remain constant, an increase in the coating speed, U, leads to a corresponding decrease in the thickness of the wet film, t_{wet} – Equation 4.2. Consequently, a smaller gap must be used to maintain the desired coating characteristics. These equations help to understand the behavior of the slot-die deposition process. Better

coatings are typically achieved with solutions that have low capillary numbers, low viscosity, high surface energy and at low coating speeds.[24]

The slot-die coater was used to deposit PTAA hole transport material and perovskite layer. The electron transport layer (PCBM) and the buffer material (BCP) were deposited by spin-coating, following the host lab's optimized procedure.[23] The silver back contact was prepared by thermal evaporation.

4.1. Optimization of PTAA layer

PTAA serves as the hole transport layer in inverted perovskite solar cells, with the primary function of efficiently transport holes (positive charge carriers) from the perovskite active layer to the electrode contact (here the fluorine tin oxide, FTO). The optimization of PTAA deposition using slot-die coating began with assembling dummy cells, comprising only PTAA and silver back contact. This approach allowed the analysis of the layer's resistance to electrons passage. By assessing their ohmic resistance using the *I-V* curve, the resistance could be calculated using Equation 2.2. The dummy cells with higher slopes (R^{-1}) indicate lower resistance, which is desirable. The software JMP 18.0.1 was used to assist in the experimental design, optimizing resource allocation and minimizing the number of experiments needed to achieve reliable results. Parameters such as slot-die plate temperature, coating speed, gap between slot-die head and substrate, and ink concentration were evaluated, using the response surface methodology.

For the first optimization set of experiments, Table 4.1 shows the ranges of values used for each parameter under study, while Table Ap. A. 1 presents the experiments suggested by the software JMP. After performing the dummy devices with the suggested deposition conditions, the ohmic resistance was calculated from the *I-V* curves (see Figure 4.2 for the dummy cell delivering lower ohmic resistance), and feedback was provided to the software. By running the software, the optimal values for each parameter and desirability were obtained, which allowed to understand the variability over the studied range for each parameter. The prediction profile is presented in Figure 4.3.

Table 4.1. Process values and their corresponding limits for the first optimization of PTAA.

Temperature of the plate / °C	60-80
Plate speed / mm·s^{-1}	15-25
Concentration of PTAA / mg·mL^{-1}	1.5-2.0
Gap / µm	50

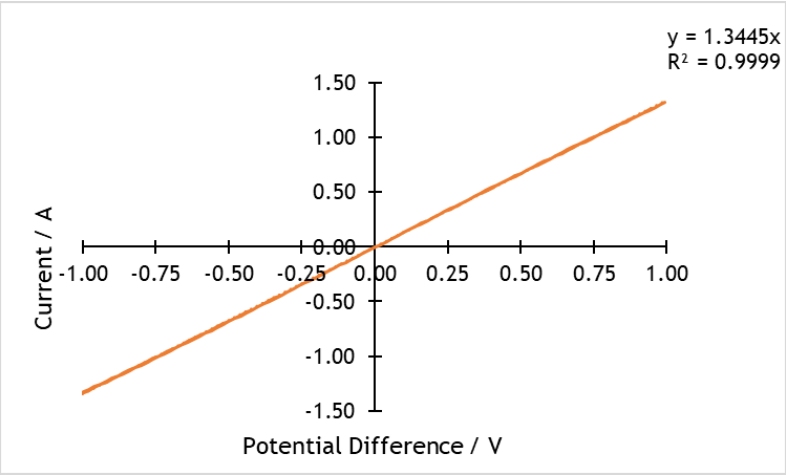


Figure 4.2. I-V characterization of the dummy cell delivering lower ohmic resistance of PTAA layer. Deposition conditions: 70 ºC *of plate temperature, 20* mm·s^{-1} coating speed, 2.00 mg·mL^{-1} of concentration of PTAA and 50 µm of gap.

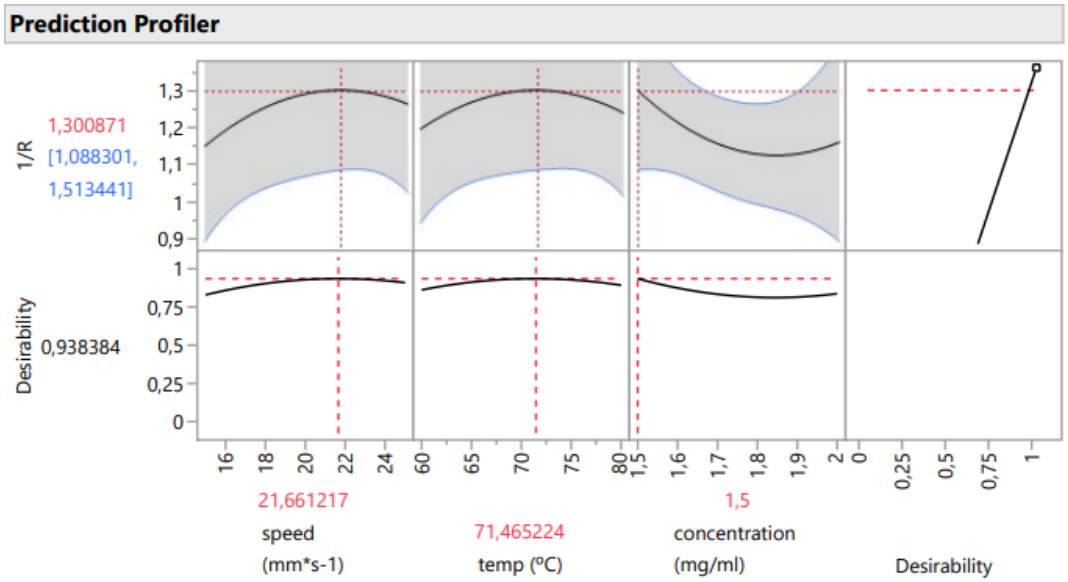


Figure 4.3. Prediction profile from JMP software for the first optimization of PTAA deposition.

Analyzing Figure 4.3, it can be observed that for a fixed gap of 50 µm, the optimal speed is 21.66 mm·s^{-1}, and the plate temperature is 71.46 ºC. In terms of concentration, the optimal value is 1.5 mg·mL^{-1}, which is the minimum value within the selected range. However, unlike the other parameters, the performance curve increases for lower concentrations. Therefore, it was necessary to explore the influence of concentrations below 1.5 mg·mL^{-1}.

A second optimization was then performed with a lower limit for the PTAA concentration and varying also the gap. The temperature was maintained at the optimal value of 70 ºC. Temperature plays an important role in the evaporation of solvent, and increases the

wettability of the substrate, allowing good surface coverage. This evaporation must be controlled to form a film without voids. Given that the gap influences the coating speed, a range of values for the gap was studied together with the study of the coating behavior at lower concentrations of PTAA. The range of parameters studied in the second optimization is presented in Table 4.2. The experiments suggested by the software and the results are presented in Table Ap. A. 2.

Table 4.2. Process values and their corresponding limits for the second optimization of PTAA.

Temperature of the plate / °C	70
Plate Speed / mm·s^{-1}	15-25
Concentration of PTAA / mg·mL^{-1}	1.25-2.00
Gap / µm	50-200

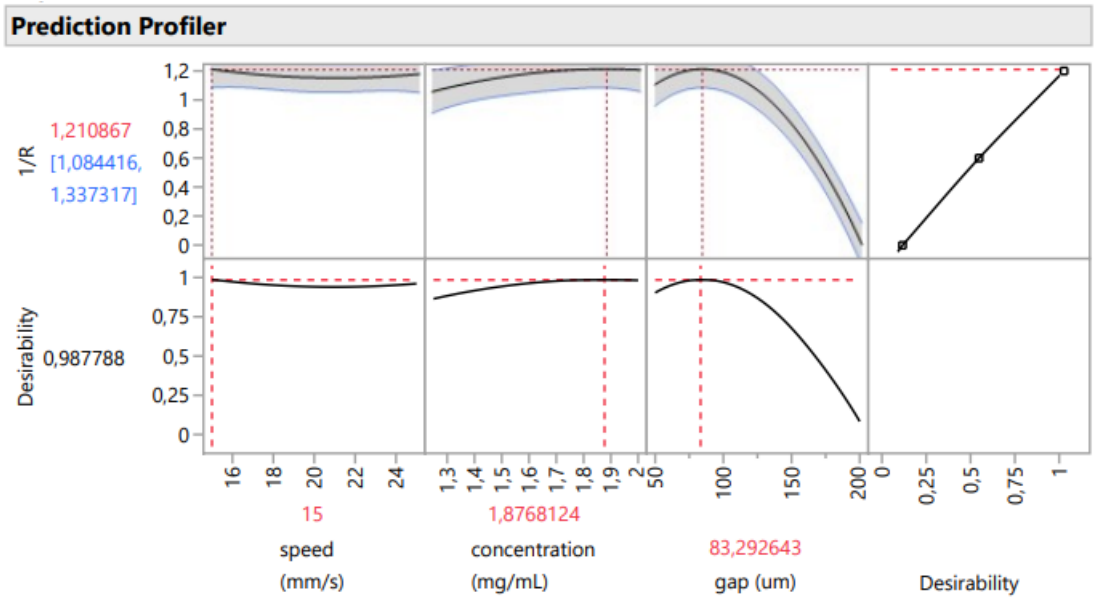


Figure 4.4. Prediction profile from JMP software for the second optimization of PTAA deposition.

An analysis of Figure 4.4 indicates that at the optimized temperature, the optimal coating speed is 15 mm·s^{-1}, the concentration is 1.88 mg·mL^{-1} and the gap is 83.3 µm. There was no significant variation in the coating speed and concentration values over the tested range, which was consistent with the previous optimization results. Regarding the gap evaluation, higher gaps and coating speeds during deposition led to increased meniscus instability. In those cases, to maintain a stable meniscus and ensure complete surface coverage, more volume of solution was required. This is explained by Equation 4.1 and Equation 4.2, which show that, for the same capillary number, a higher gap is compensated with an increase in the wet film thickness.

This can be achieved by increasing the volume of solution used or by decreasing the coating speed. For experiments with higher gaps (H_0 > 125 µm), to form a stable meniscus it was necessary to increase the volume of PTAA solution. Since PTAA is an expensive material, this range of values becomes less economically feasible.

Based on these results, the best PTAA deposition conditions were tested in full devices, because having a low resistance does not guarantee that the film is uniform or has the ideal thickness for efficient hole transport. SEM characterization cannot be used to directly analyze the morphology of the deposited film because the PTAA layer is colorless and a very thin film.

To fabricate the complete devices, perovskite layer was also deposited using slot-die coating instead of the usual spin-coating. This choice was made to anticipate certain challenges associated with perovskite deposition by slot-die coating, even if its full optimization will be done next. Typically, the spin-coating process uses DMF as the perovskite precursor solvent. However, due to its high boiling point and the need for an antisolvent process to assist crystallization, this solvent system is not adequate for slot-die deposition. Consequently, solvents with lower boiling points, such as ACN and MA(MeOH), are employed. Low boiling point solvents eliminate the need for antisolvents to assist perovskite crystallization, as the temperature-induced evaporation of solvents initiates crystal growth.[17] From an industrial point of view, avoiding antisolvent-assisted crystallization is also of great importance as it eliminates the operator influence in the assembly, enhancing reproducibility. Since the PTAA layer is hydrophobic, it is necessary to increase the wettability of the substrate to allow the perovskite solution to spread properly. For this purpose, the slot-die plate was heated. [17]

After preparing and characterizing the full inverted PSC devices, it was noticed that all the cells were short-circuited. Indeed, achieving working PSCs necessitates a uniform film and well-developed crystals. To determine the causes of these short-circuits, the morphology of the cells was analyzed using SEM characterization. Figure 4.5 shows the SEM images showing the surface morphology of the cells.

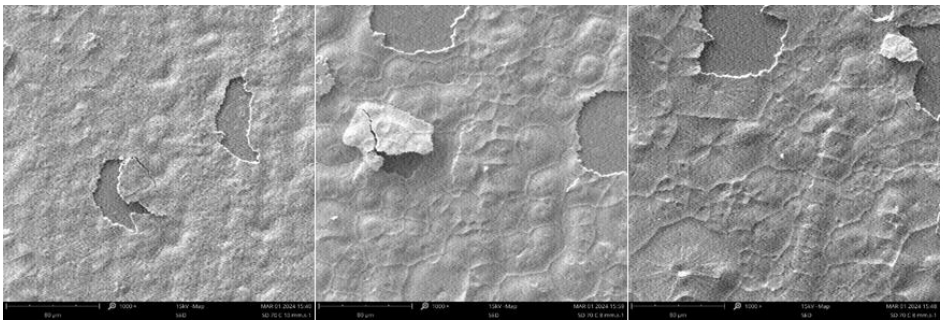


Figure 4.5. Top-view images of the surface morphology of the perovskite layer using SEM characterization.

After analyzing these images, it was concluded that there is material removed from the surface. This material was the perovskite layer, resulting in the formation of large voids in the film, allowing the PTAA to contact the PCBM, therefore creating a direct pathway for charge carriers and leading to a short-circuit in the cell. For solving this issue, it was needed to first ensure adequate perovskite crystallization. For that, the influence of the temperature of the slot-die plate and sintering were studied to achieve a void-free perovskite layer, as the voids appear after the perovskite crystallization with the temperature being the only variable. Each of these parameters, presented in Table 4.3, has a distinct impact on the perovskite layer deposition and correspondent crystallization.

Table 4.3. Range of temperatures studied.

Slot-die plate temperature / ºC	35, 40, 50, 60, 70, 80
Sintering temperature / ºC	80, 100

For the cell function properly, the perovskite film must be uniform and well-crystallized with large crystals. Figure 4.6 shows that at lower slot-die plate temperatures, smaller crystals are formed, but increasing the temperature of the slot-die plate results in larger crystals. However, at 80 ºC more voids are observed compared to other temperatures. So, it is possible to conclude that 70 ºC is the optimal temperature for the best perovskite film crystallization.

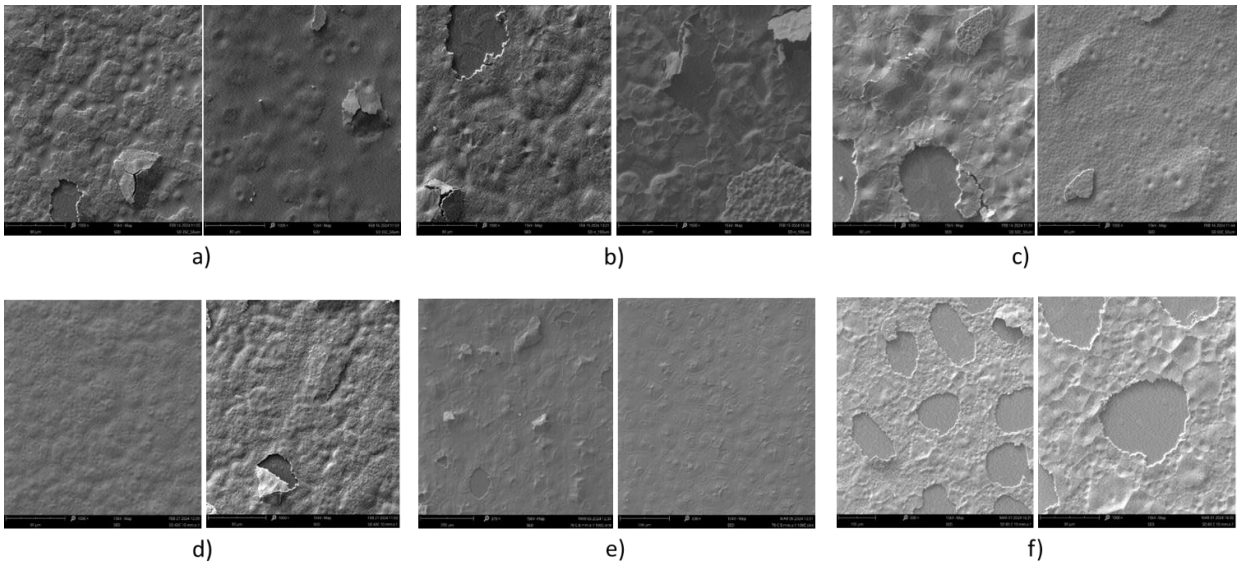


Figure 4.6. SEM images of perovskite layer using a sintering temperature of 100 ºC and different slot-die plate temperatures: a) 35 ºC, b) 40 ºC, c) 50 ºC, d) 60 ºC, e) 70 ºC, f) 80 ºC.

To evaluate the sintering temperature, a slot-die plate temperature of 70 ºC was used in both cases and the SEM images are shown in Figure 4.7. It is possible to observe that no voids were observed at a sintering temperature of 80 ºC, whereas at 100 ºC many voids were seen. So, it is possible to conclude that these voids were caused by the higher sintering temperature, which led to rapid solvent evaporation.

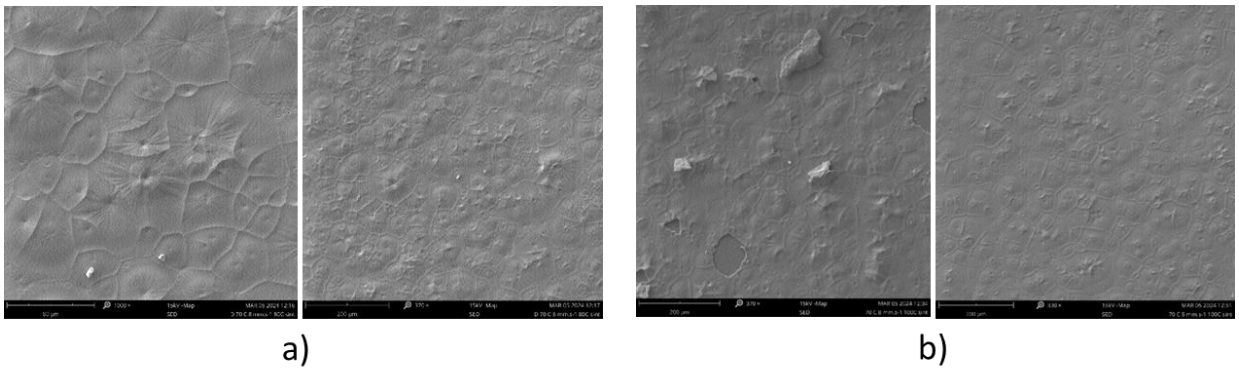


Figure 4.7. SEM images of the perovskite layer using different sintering temperatures: a) 80 ºC, b) 100 ° C.

The slot-die plate temperature directly influences the crystallization of the perovskite film. With a perovskite film free of voids, it is now feasible to fabricate fully functional devices using a slot-die plate temperature of 70 ºC and a sintering temperature of 80 ºC.

With a reasonable perovskite deposition quality, full inverted PSC devices were prepared using the two optimal conditions provided by the JMP software optimization for the PTAA deposition

using slot-die coating (Conditions 2 and 3 in Table 4.4). Additionally, another set of deposition conditions was tested, specifically the conditions that resulted in the lowest ohmic resistance when dummy cells were assembled – Figure 4.2. This condition is labeled as Condition 1 in Table 4.4. Figure 4.8 presents the principal photovoltaic parameters of the PSC cells prepared.

Table 4.4. Conditions of PTAA used for preparing full PSC devices.

Condition 1	Condition 2	Condition 3
Concentration: 2 mg·mL^{-1}	Concentration: 1.5 mg·mL^{-1}	Concentration: 1.88 mg·mL^{-1}
Speed: 20 mm·s^{-1}	Speed: 21.66 mm·s^{-1}	Speed: 15 mm·s^{-1}
Gap: 50 µm	Gap: 50 µm	Gap: 85 µm
Temperature: 70 ºC	Temperature: 70 ºC	Temperature: 70 ºC

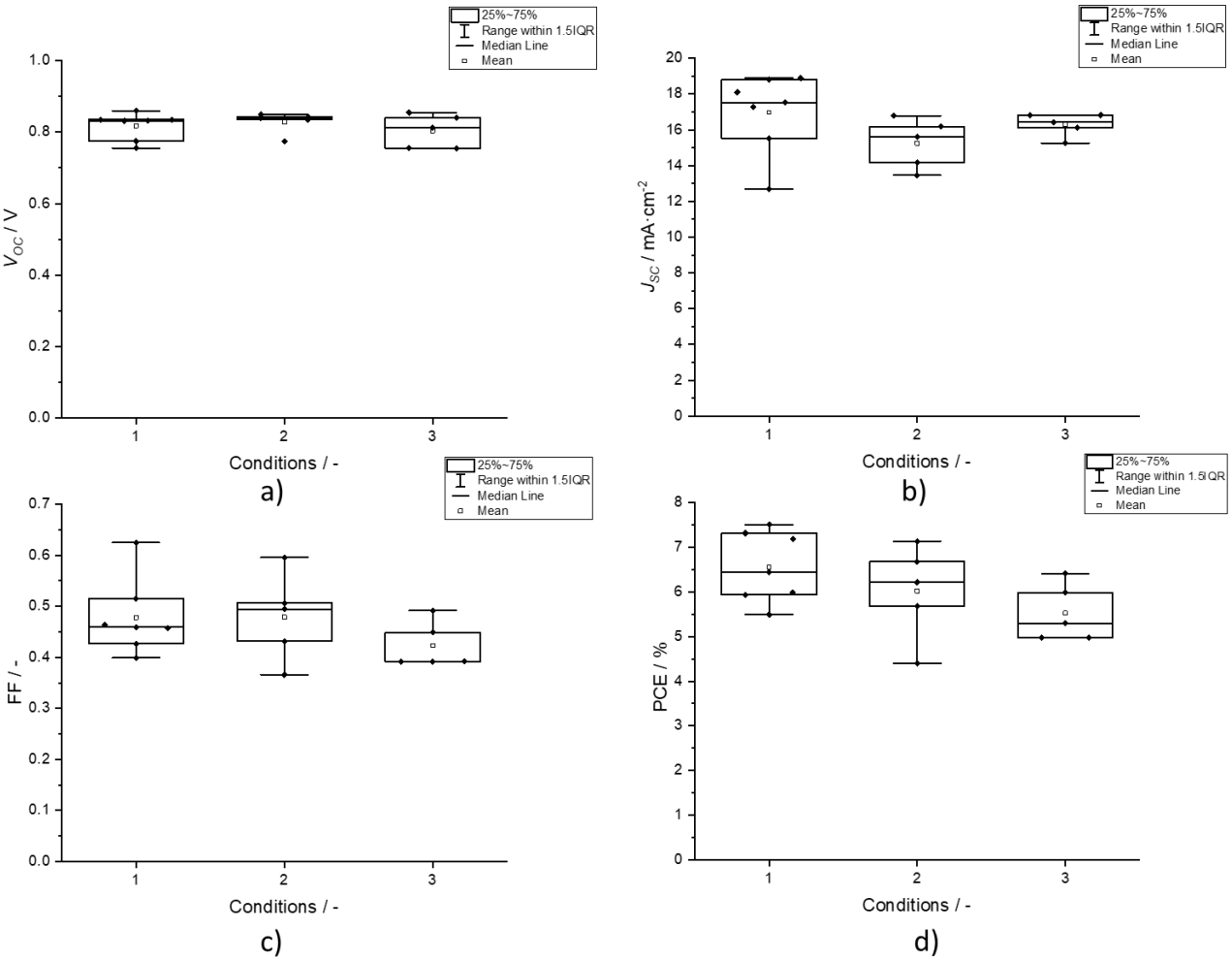


Figure 4.8. Photovoltaic performance parameters of the PSC devices prepared based on the three selected conditions for the PTAA slot-die deposition: a) V_{OC}, b) J_{SC}, c) FF, d) PCE.

From the analysis of Figure 4.8, it was observed that conditions 1 and 2 exhibit very similar photovoltaic parameters, while condition 3 shows significantly poorer performance. The analysis demonstrated that the champion device was obtained for condition 1 with good reproducibility: 7.51 %, 0.83 V, 17.53 mA·cm^{-2} and *FF* of 0.52.

4.2. Optimization of perovskite layer

After finding the optimal condition for the PTAA layer, the perovskite layer was optimized using complete devices. Using the *I-V* curve, the *PCE* can be calculated using Equation 2.4 and Equation 2.5. The software JMP was used to assist in the design of performed experiments. Table 4.5 presents the ranges of values used for each parameter evaluated. The suggested experiments by the software and corresponding results are shown in Table Ap. A. 3. After performing the complete devices with the suggested deposition conditions, the PCE was calculated (Figure 4.9), and feedback was provided to the software (Figure 4.10).

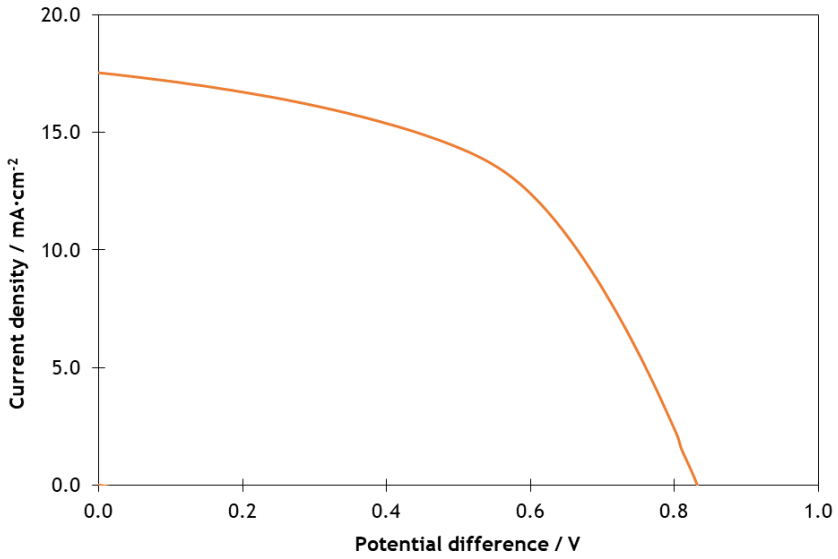


Figure 4.9. I-V curve for a complete PSC device. Deposition conditions: 70 ºC for the slot-die plate temperature, 80 ºC for sintering temperature, 10 mm·s^{-1} coating speed, 1.1 mol·L^{-1} of perovskite concentration and 50 µm Gap.

Table 4.5. Process values and their corresponding ranges for the perovskite slot-die deposition optimization.

Temperature of the slot-die plate / °C	70
Coating Speed / mm·s^{-1}	8-25
Concentration of perovskite / mg·mL^{-1}	0.75-1.25
Gap / µm	50-200

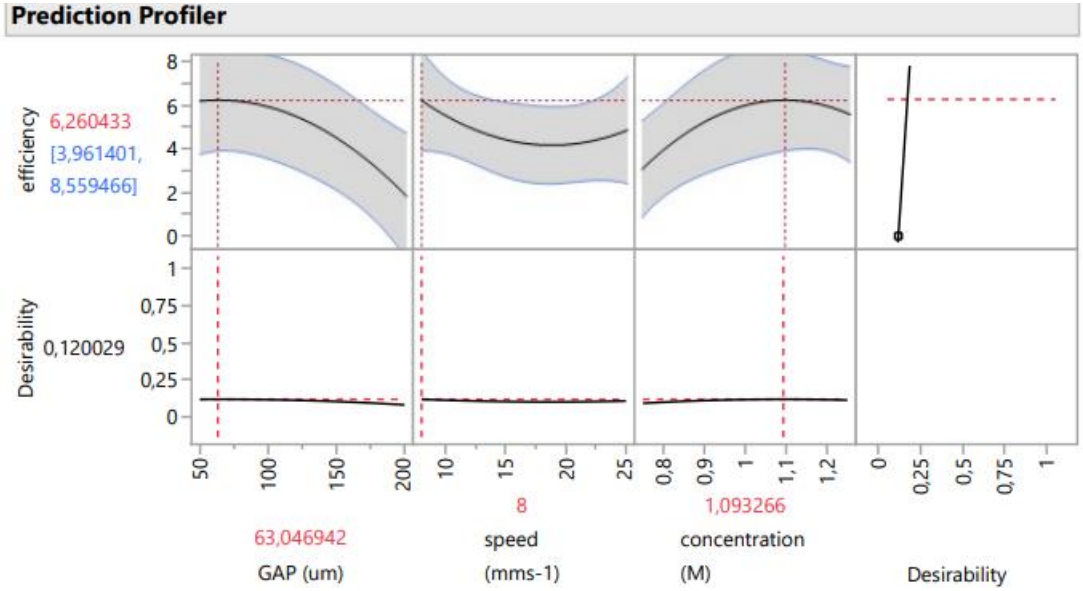


Figure 4.10. Prediction profile from JMP software for the perovskite optimization.

An analysis of Figure 4.10 reveals that the optimal coating speed is 8 mm·s^{-1}, the concentration of perovskite solution is 1.09 mol·L^{-1}, and the gap is 63.05 µm. Significant variations were observed in coating speed, ink concentration and gap across the range values tested. Lower concentrations resulted in a non-compact perovskite film and smaller crystals, which increased electron recombination and reduced current density. Regarding the gap, instability of the meniscus was observed at higher values, ≥125 µm, making it difficult to deposit the layer uniformly across the substrate. This behavior mirrors observations made during PTAA optimization. Indeed, as explained by Equation 4.1 and Equation 4.2, a higher gap requires increasing the wet film thickness, the volume of solution used, or decreasing the coating speed. Since the coating speed varied, it was necessary to increase the volume of solution used. For gaps larger than 200 µm, it was observed that even with an increased volume of solution, the meniscus did not remain stable.

SEM characterization was essential for analyzing the morphology and thickness of the perovskite film. In Appendix C, top-view and cross-sectional SEM images are presented to aid in characterizing the films under the conditions specified in Table Ap. A. 3. These images facilitate the analysis of defects inherent to the deposition process, as explained in Figure 2.7. Across all deposition conditions tested, the most prevalent defect observed was ribbing, which becomes more pronounced at higher values of coating speed and gap. In contrast, lower coating speeds and gaps lead to more uniform films with less variation in thickness across the deposition area. Air entrainment defects are particularly evident at higher gap values, and increasing the coting speed exacerbates their occurrence in the perovskite film. The relationship between the coating conditions and these defects is detailed in Table 4.6.

Table 4.6. Relationship between the coating conditions used and defects observed.

Coating conditions	Defects
High coating speed and high gap	Lots of air entrainment and ribbing
High coating speed and low gap	Some ribbing
Low coating speed and high gap	Some air entrainment and ribbing
Low coating speed and low gap	Slight ribbing

Following, the coating conditions that can lead to higher efficiencies were determined. The main photovoltaic parameters are presented in Figure 4.11 and Table Ap. B. 2.

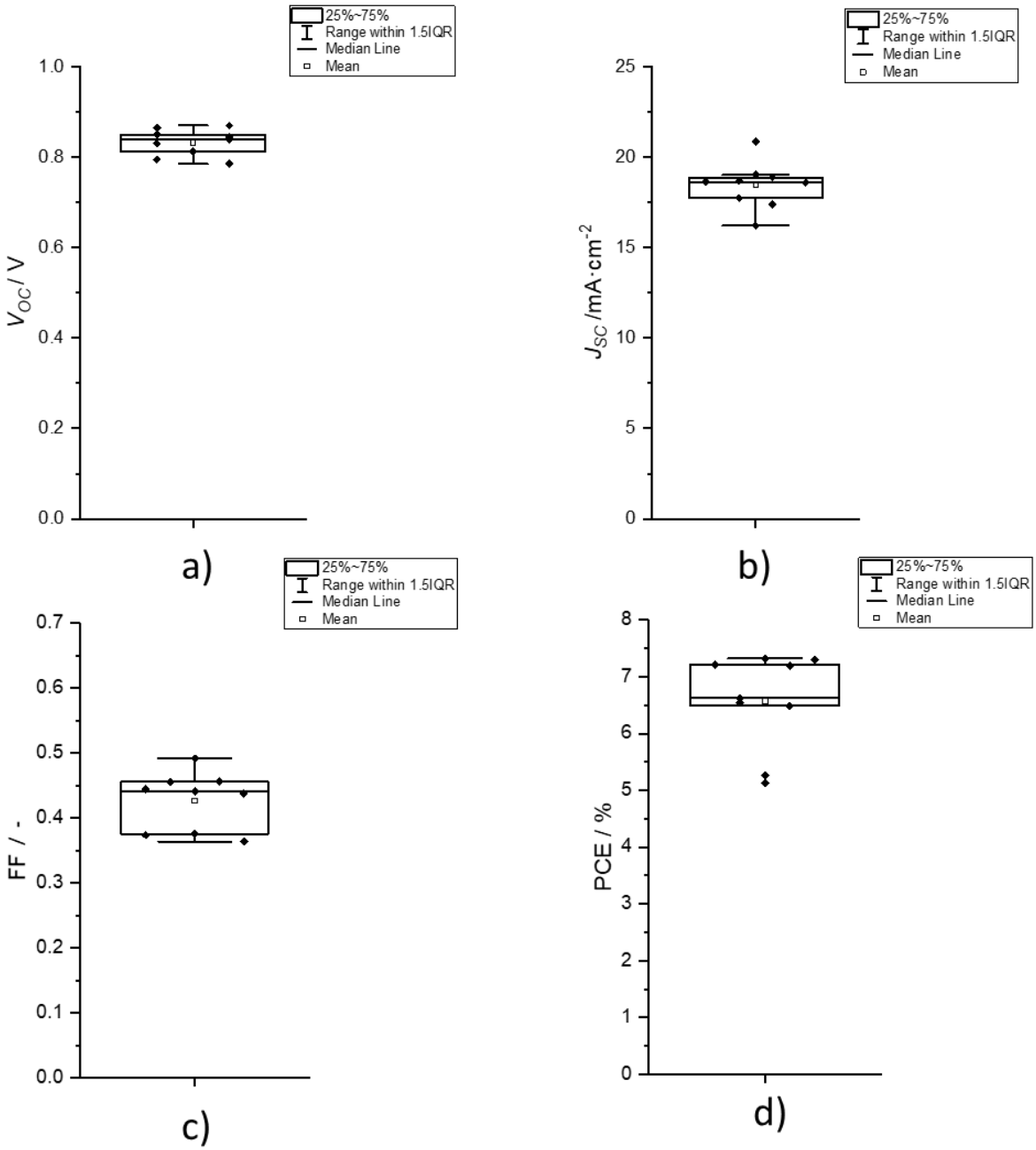
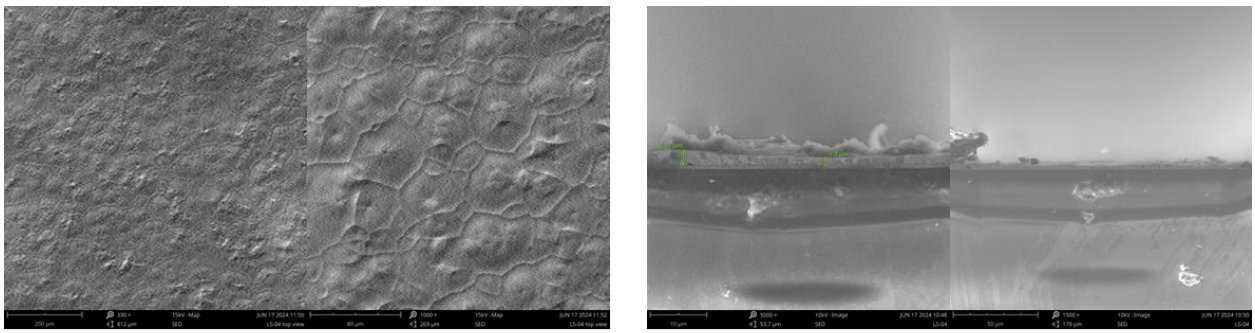


Figure 4.11. Photovoltaic performance parameters of the PSC devices prepared with the optimal conditions obtained with optimized perovskite slot-die deposition: a) V_{OC}, b) J_{SC}, c) FF*, d)* PCE.

Figure 4.11 demonstrates good reproducibility in the slot-die coating process, which relies more on equipment precision than operator skills. The average V_{OC} was 0.83 V, Figure 4.11a, indicating some energy mismatch in the interface active layer that affects device performance. The average J_{SC} was 18.86 mA·cm^{-2}, Figure 4.11b, suggesting effective crystallization of the perovskite film and good uniformity. The *FF*, slightly below 0.5, Figure 4.11c, may be attributed to structural defects within the device but is typical for larger devices due to increased

substrate series resistance (here 5 cm^2). The average PCE was 6.96 %, Figure 4.11d, highlighting the champion device performance reaching 7.32 % PCE (0.85 V, 18.88 $mA \cdot cm^{-2}$ and *FF* of 0.46).

Using SEM characterization, it was possible to compare the images in Appendix C with those of the PSC device prepared under optimized conditions, and which are presented in Figure 4.12. Analysis of this image reveals that the film exhibits good crystallization and uniformity, and it is relatively thin, with approximately (1.855 ± 0.555) µm. The film is highly compact, showing minimal thickness variations and no air entrainment.



a) b)

Figure 4.12: SEM images of PSC device prepared with optimized slot-die coating conditions: a) top-view, and b) cross-section.

In order to analyze the uniformity of the deposition along the substrate, a PSC device was divided into 3 smaller cells using the laser ablation system- Figure 4.13.

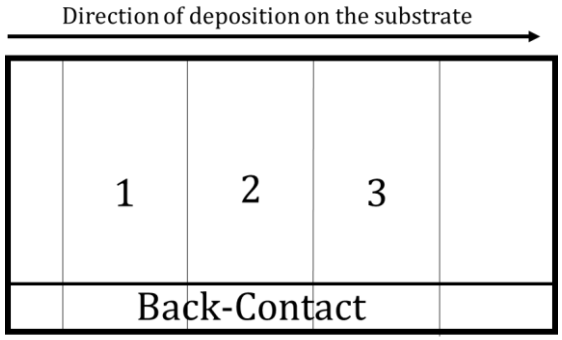
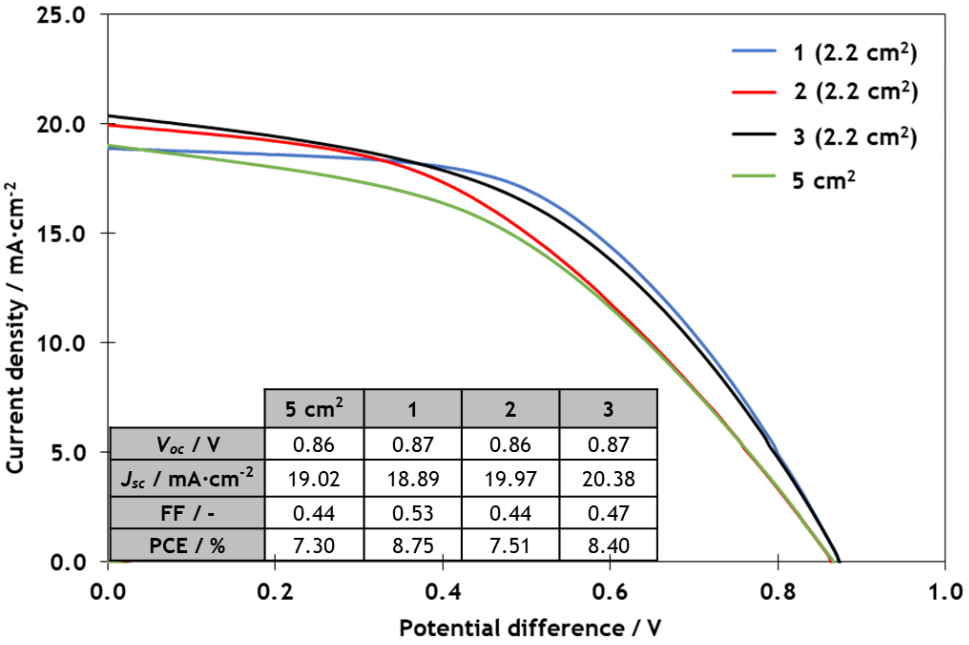


Figure 4.13. PSC device divided into 3 small cells to evaluate the quality of the slot-die coating deposition.

Figure 4.14 displays the *I-V* curves for both the 5 cm^2 device and its segmented parts. Analysis of these curves reveals that each segmented part exhibits slightly superior performance compared to the 5 cm^2 device, as expected since it is characterizing a smaller area with likely fewer defects.[25] This analysis is crucial for evaluating the shunt resistance and series

resistance in each segmented part in order to assess the quality of layers deposition. An ideal device will have a fill factor equal to 1. However, due to the presence of shunt and series resistances, there is a loss of current density along the electrical circuit analogue, attributed to recombination or poor contact between the layers –Figure 2.11. Low shunt resistance results in a decrease in current density at high potential differences, whereas high series resistance leads to a reduced current density at low potential differences. Optimal device performance requires a high shunt resistance and low series resistance, ideally achieving a *FF* close to 1.[18]



	5 cm²	1	2	3
V_{oc} / V	0.86	0.87	0.86	0.87
J_{sc} / mA·cm^{-2}	19.02	18.89	19.97	20.38
FF / -	0.44	0.53	0.44	0.47
PCE / %	7.30	8.75	7.51	8.40

Figure 4.14. Current Density - potential difference curve for a full PSC device (5 cm^2) and its segmented parts (2.2 cm^2).

At the beginning of the substrate (Zone 1), there is a decrease in series resistance and an increase in shunt resistance, resulting in higher FF and improved PCE. This suggests fewer defects and lower recombination of charges. In the intermediate section (Zone 2) and in the final section of the substrate (Zone 3), the behavior resembles that of the 5 cm^2 device, although with a higher current, possibly due to better perovskite crystallization. Zone 3 has a higher shunt resistance when compared with the 5 cm^2 device, resulting in a higher FF and higher PCE. In conclusion, it can be stated that the substrate underwent uniform deposition because all segmented parts exhibited comparable PCE.After optimizing PTAA and perovskite layers deposition using slot-die coating, a bench marketing between our results and those reported in existing literature should be conducted. Annex A includes two tables, Table An. A 1 and Table An. A 2, which presents the efficiencies of devices where at least the perovskite

layer was deposited using slot-die coating, produced under ambient air and in a controlled atmosphere, respectively. Figure 4.15 displays the values from these tables alongside the result obtained in this work: 7.32 % with an active area of 5 cm^2.

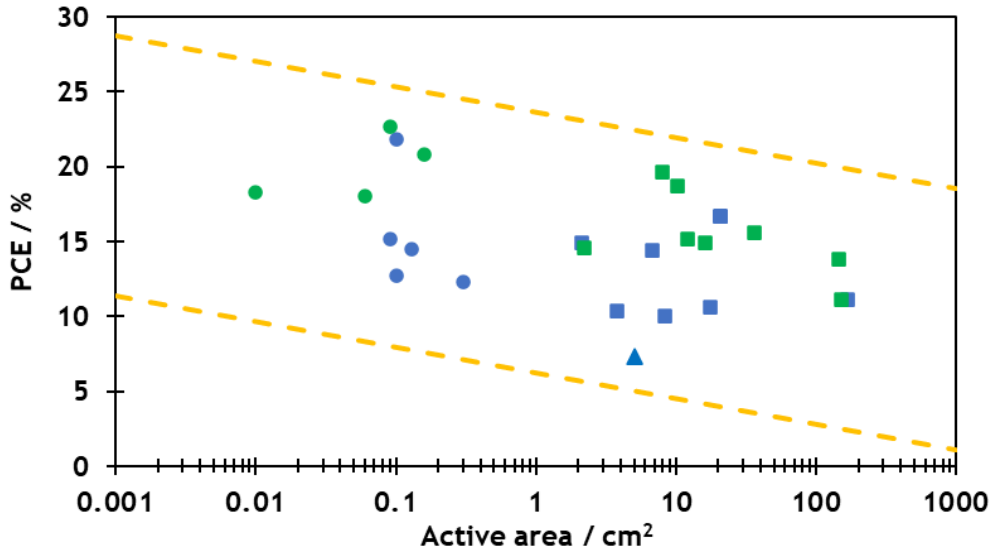


Figure 4.15. PCE of PSC devices prepared using slot-die coating (at least the perovskite layer) as a function of the active area. Individual solar cells are represented by circles and modules are represented by squares. The blue color refers to devices produced under ambient air and the green color to devices made in a controlled atmosphere. The best-performing PSC device obtained based on this work is represented with a triangle. Adapted from ref. [25].

The increase in active area results in decreased efficiency, as indicated by the yellow dashed lines. This trend has been documented in previous studies. [25] Devices manufactured in ambient air demonstrate inferior performance compared to those produced in a controlled atmosphere. When compared to results reported in the literature, the champion device developed in this work falls below the reported values. It is important to note, however, that the device size range used in this study falls within the region where module results are typically presented, which makes direct comparison less equitable due to the influence of increased area on final performance. Moreover, the perovskite material used in this study features a simple structure and stability under ambient conditions, but additional structural modifications could enhance light absorption efficiency. Further optimization is needed for the other active layers to achieve a fully slot-die coated device.

5. Conclusion

To reduce dependency on fossil fuels, renewable energies have emerged as a viable alternative. Solar energy, in particular, has experienced rapid development driven by increased investment in the sector. The introduction of perovskite solar cells has significantly advanced the field of solar cells due to their characteristics and the ability to deposit them in both flexible and rigid substrates, approaching efficiencies of silicon-based solar cells. Among the various technologies for thin-film deposition available, this work focused on the slot-die coating, known for its advantages in scaling up and implementing roll-to-roll processing (deposition on a roll of flexible plastic).

This study aimed at two main objectives: optimizing the PTAA layer deposition using a slot-die coater and subsequently the perovskite layer deposition. The optimized conditions for the PTAA layer were as follows: coating speed of 20 $mm \cdot s^{-1}$, gap of 50 µm between the slot-die head and the substrate, slot-die plate temperature of 70 ºC, sintering temperature of 100 ºC and PTAA concentration of 2 $mg \cdot mL^{-1}$. For the perovskite layer, the optimal conditions were: coating speed of 8 $mm \cdot s^{-1}$, gap of 65 µm, slot-die plate temperature of 70 ºC, sintering temperature of 80 ºC and a perovskite precursor concentration of 1.1 $mol \cdot L^{-1}$.

The highest efficiency achieved for a PSC prepared with these optimized conditions was 7.32 % for an active area of 5 cm^2. The PSC device was then divided into three parts to analyze the uniformity of the deposition. Zone 1 presented higher FF but lower current, whereas Zones 2 and 3 showed lower FF but higher current. This led to an improved efficiency of 8.75 % for an active area of 2.2 cm^2 corresponding to Zone 1. Indeed, for this evaluation of efficiency throughout the cell deposition process, it was observed that while the efficiency remained relatively stable, there were variations in shunt and series resistance as well as in current density generation.

When compared to the literature values for the same coating technique, the results of this work are slightly lower but still within an acceptable range. This indicates that while promising, there is room for improvement.

Future work should focus on several modifications to further enhance efficiency. These include altering the perovskite structure, incorporating additives to increase humidity stability, using a gas knife to improve crystallization during the deposition, optimizing the slot-die deposition for the PCBM layer and doing a morphological analysis by dividing the substrate to understand the optimal substrate size for module fabrication. These efforts aim to contribute to the overall advancement of perovskite solar cell technology.

6. Assessment of the work done

6.1. Objectives Achieved

This study represents the first exploration of slot-die deposition within the host laboratory. Thus, the primary objective was to optimize the deposition of the active layers, mainly envisaging deposition under ambient conditions. For that, a simple $MAPbI_3$ perovskite structure was selected. It was successfully deposited by slot-die coating the PTAA and perovskite layers, while PCBM and BCP were deposited by spin-coater. Future work will focus on the optimization of these remaining layers, and adapt the deposition of the perovskite to more complex structures but with enhanced efficiency, aiming to fulfil the project's ultimate objectives.

6.2. Contribution to the Sustainable Development Goals

ODS	Targets	Contribution	Performance indicators and metrics
7	7.1	Ensure universal access to modern, reliable and affordable energy services	Perovskite solar cells can be produced at a lower cost compared to traditional silicon-based solar cells, which can contribute to the widespread of solar technologies and make them more affordable and accessible
	7.2	Increase renewable energy share in the total final energy consumption	The major advances in the efficiency of perovskite solar cells, combined with their low-cost production and the versatility of applications, make them a good candidate for revolutionizing the photovoltaic market and offer great potential for meeting the world's energy needs.
	7.3	Double the overall rate of energy efficiency improvement	Perovskite solar cells can be integrated into buildings as an energy-efficient solution to turn them into decentralized energy producers. In addition, as an off-grid energy system, perovskite solar cells offer an excellent opportunity for developing countries to reduce inequality between urban and rural areas, as electricity can be provided in a short time, people do not have to wait several years to be connected to the national grid.

13	13.2	Reduction of the total greenhouse gas emissions per year	Photovoltaic technologies are sustainable and clean energy sources with less pollution during their lifetime compared to other renewable energy sources. In particular, perovskite solar cells use abundant raw materials and low-energetic demanding fabrication processes, leading to a low carbon footprint and environmental impact even when compared to silicon panels.

6.3. Final Assessment

This project had a very positive impact, as it facilitated the development of important research skills and provided valuable laboratory experience. It was challenging due to various obstacles encountered along the way, both at the project and personal levels, which fostered resilience and enhanced problem-solving abilities. Additionally, it provided an opportunity to explore new domains of engineering, particularly thin-film deposition techniques.

7. References

[1] IEA. "Renewables 2023." https://www.iea.org/reports/renewables-2023 (accessed March 2024.

[2] IEA. "Annual investment in fossil fuels and clean energy, 2015-2023." https://www.iea.org/data-and-statistics/charts/annual-investment-in-fossil-fuels-and-clean-energy-2015-2023 (accessed March 2024.

[3] Y. Tu, J. Ye, G. Yang, Y. Zang, L. Zhang, Y. Wang, G. Li, L. Chu, and W. Yan, "Slot-die coating fabrication of perovskite solar cells toward commercialization," *Journal of Alloys and Compounds,* vol. 942, p. 169104, 2023.

[4] N. R. E. Laboratory. "Best Research-Cell Efficiency Chart." https://www.nrel.gov/pv/cell-efficiency.html (accessed March 2024.

[5] H. Hu, "The fabrication, characterization and simulation of inverted perovskite solar cells," 2019.

[6] Y. Bai, "Materials and interface design for high-performance perovskite solar cells with an inverted structure," 2017.

[7] Y.-C. Huang, C.-F. Li, Z.-H. Huang, P.-H. Liu, and C.-S. Tsao, "Rapid and sheet-to-sheet slot-die coating manufacture of highly efficient perovskite solar cells processed under ambient air," *Solar Energy,* vol. 177, pp. 255-261, 2019.

[8] A. Mishra, M. A. Hope, M. Grätzel, and L. Emsley, "A Complete Picture of Cation Dynamics in Hybrid Perovskite Materials from Solid-State NMR Spectroscopy," *Journal of the American Chemical Society,* vol. 145, no. 2, pp. 978-990, 2023/01/18 2023, doi: 10.1021/jacs.2c10149.

[9] F. F. Targhi, Y. S. Jalili, and F. Kanjouri, "MAPbI3 and FAPbI3 perovskites as solar cells: Case study on structural, electrical and optical properties," *Results in physics,* vol. 10, pp. 616-627, 2018.

[10] S. H. Huang, C. K. Guan, P. H. Lee, H. C. Huang, C. F. Li, Y. C. Huang, and W. F. Su, "Toward all slot-die fabricated high efficiency large area perovskite solar cell using rapid near infrared heating in ambient air," *Advanced Energy Materials,* vol. 10, no. 37, p. 2001567, 2020.

[11] Y. Rong, Y. Ming, W. Ji, D. Li, A. Mei, Y. Hu, and H. Han, "Toward industrial-scale production of perovskite solar cells: screen printing, slot-die coating, and emerging techniques," *The Journal of Physical Chemistry Letters,* vol. 9, no. 10, pp. 2707-2713, 2018.

[12] X. Ding, J. Liu, and T. A. Harris, "A review of the operating limits in slot die coating processes," *AIChE Journal,* vol. 62, no. 7, pp. 2508-2524, 2016.

[13] E. B. Creel, K. Tjiptowidjojo, J. A. Lee, K. M. Livingston, P. R. Schunk, N. S. Bell, A. Serov, and D. L. Wood III, "Slot-die-coating operability windows for polymer electrolyte membrane fuel cell cathode catalyst layers," *Journal of Colloid and Interface Science,* vol. 610, pp. 474-485, 2022.

[14] L. Sartor, *Slot coating: fluid mechanics and die design*. University of Minnesota, 1990.

[15] D. Lee, Y.-S. Jung, Y.-J. Heo, S. Lee, K. Hwang, Y.-J. Jeon, J.-E. Kim, J. Park, G. Y. Jung, and D.-Y. Kim, "Slot-die coated perovskite films using mixed lead precursors for highly reproducible and large-area solar cells," *ACS applied materials & interfaces,* vol. 10, no. 18, pp. 16133-16139, 2018.

[16] E. Bi, W. Tang, H. Chen, Y. Wang, J. Barbaud, T. Wu, W. Kong, P. Tu, H. Zhu, and X. Zeng, "Efficient perovskite solar cell modules with high stability enabled by iodide diffusion barriers," *Joule,* vol. 3, no. 11, pp. 2748-2760, 2019.

[17] A. S. Subbiah, F. H. Isikgor, C. T. Howells, M. De Bastiani, J. Liu, E. Aydin, F. Furlan, T. G. Allen, F. Xu, and S. Zhumagali, "High-performance perovskite single-junction and textured perovskite/silicon tandem solar cells via slot-die-coating," *ACS Energy Letters,* vol. 5, no. 9, pp. 3034-3040, 2020.

[18] C. B. H. a. S.G.Bowden. "Photovoltaics Education Website." www.pveducation.org (accessed May, 2024).

[19] Ossila. "Slot Die Coater." https://www.ossila.com/products/slot-die-coater (accessed 20/06/2024, 2024).

[20] Polos. "Spin Coaters." https://www.sps-polos.com/en/webshop/webshop/coating/spin-coaters/ (accessed 20/06/2024, 2024).

[21] "Bench-top High Vacuum and Thin Film Products." http://www.oxford-vacuum.com/ (accessed 20/06/2024, 2024).

[22] T. Scientific. "Phenom ParticleX Steel Desktop SEM." https://www.thermofisher.com/order/catalog/product/PARTICLEX-STEEL?SID=srch-srp-PARTICLEX-STEEL (accessed 20/06/2024, 2024).

[23] J. Príncipe, V. C. Duarte, A. l. Mendes, and L. s. Andrade, "Influence of the Transparent Conductive Oxide Type on the Performance of Inverted Perovskite Solar Cells," *ACS Applied Energy Materials,* vol. 6, no. 24, pp. 12442-12451, 2023.

[24] C. Teixeira, R. Fuentes-Pineda, L. Andrade, A. Mendes, and D. Forgács, "Fabrication of low-cost and flexible perovskite solar cells by slot-die coating for indoor applications," *Materials Advances,* vol. 4, no. 17, pp. 3863-3873, 2023.

[25] D. B. Ritzer, T. Abzieher, A. Basibüyük, T. Feeney, F. Laufer, S. Ternes, B. S. Richards, S. Bergfeld, and U. W. Paetzold, "Upscaling of perovskite solar modules: The synergy of fully evaporated layer fabrication and all-laser-scribed interconnections," *Progress in Photovoltaics: Research and Applications,* vol. 30, no. 4, pp. 360-373, 2022.

[26] Y. Galagan, F. Di Giacomo, H. Gorter, G. Kirchner, I. de Vries, R. Andriessen, and P. Groen, "Roll-to-roll slot die coated perovskite for efficient flexible solar cells," *Advanced Energy Materials,* vol. 8, no. 32, p. 1801935, 2018.

[27] J.-E. Kim, Y.-S. Jung, Y.-J. Heo, K. Hwang, T. Qin, D.-Y. Kim, and D. Vak, "Slot die coated planar perovskite solar cells via blowing and heating assisted one step deposition," *Solar Energy Materials and Solar Cells,* vol. 179, pp. 80-86, 2018.

[28] A. Vijayan, M. B. Johansson, S. Svanström, U. B. Cappel, H. k. Rensmo, and G. Boschloo, "Simple method for efficient slot-die coating of MAPbI3 perovskite thin films in ambient air conditions," *ACS Applied Energy Materials,* vol. 3, no. 5, pp. 4331-4337, 2020.

[29] T. S. Le, D. Saranin, P. Gostishchev, I. Ermanova, T. Komaricheva, L. Luchnikov, D. Muratov, A. Uvarov, E. Vyacheslavova, and I. Mukhin, "All-Slot-Die-Coated Inverted Perovskite Solar Cells in Ambient Conditions with Chlorine Additives," *Solar RRL,* vol. 6, no. 2, p. 2100807, 2022.

[30] L. Cai, L. Liang, J. Wu, B. Ding, L. Gao, and B. Fan, "Large area perovskite solar cell module," *Journal of Semiconductors,* vol. 38, no. 1, p. 014006, 2017.

[31] Z. Yang, W. Zhang, S. Wu, H. Zhu, Z. Liu, Z. Liu, Z. Jiang, R. Chen, J. Zhou, and Q. Lu, "Slot-die coating large-area formamidinium-cesium perovskite film for efficient and stable parallel solar module," *Science Advances,* vol. 7, no. 18, p. eabg3749, 2021.

[32] F. Di Giacomo, S. Shanmugam, H. Fledderus, B. J. Bruijnaers, W. J. Verhees, M. S. Dorenkamper, S. C. Veenstra, W. Qiu, R. Gehlhaar, and T. Merckx, "Up-scalable sheet-to-sheet production of high efficiency perovskite module and solar cells on 6-in. substrate using slot die coating," *Solar Energy Materials and Solar Cells,* vol. 181, pp. 53-59, 2018.

[33] Y. Y. Kim, E. Y. Park, T.-Y. Yang, J. H. Noh, T. J. Shin, N. J. Jeon, and J. Seo, "Fast two-step deposition of perovskite via mediator extraction treatment for large-area, high-performance perovskite solar cells," *Journal of Materials Chemistry A,* vol. 6, no. 26, pp. 12447-12454, 2018.

[34] J. B. Whitaker, D. H. Kim, B. W. Larson, F. Zhang, J. J. Berry, M. F. Van Hest, and K. Zhu, "Scalable slot-die coating of high performance perovskite solar cells," *Sustainable Energy & Fuels,* vol. 2, no. 11, pp. 2442-2449, 2018.

[35] M. Du, X. Zhu, L. Wang, H. Wang, J. Feng, X. Jiang, Y. Cao, Y. Sun, L. Duan, and Y. Jiao, "High-pressure nitrogen-extraction and effective passivation to attain highest large-area perovskite solar module efficiency," *Advanced Materials,* vol. 32, no. 47, p. 2004979, 2020.

[36] J. Li, J. Dagar, O. Shargaieva, M. A. Flatken, H. Köbler, M. Fenske, C. Schultz, B. Stegemann, J. Just, and D. M. Többens, "20.8% slot-die coated MAPbI3 perovskite solar cells by optimal DMSO-content and age of 2-ME based precursor inks," *Advanced Energy Materials,* vol. 11, no. 10, p. 2003460, 2021.

[37] I. Zimmermann, M. Al Atem, O. Fournier, S. Bernard, S. Jutteau, L. Lombez, and J. Rousset, "Sequentially slot-die-coated perovskite for efficient and scalable solar cells," *Advanced Materials Interfaces,* vol. 8, no. 18, p. 2100743, 2021.

[38] T. Bu, J. Li, F. Zheng, W. Chen, X. Wen, Z. Ku, Y. Peng, J. Zhong, Y.-B. Cheng, and F. Huang, "Universal passivation strategy to slot-die printed SnO2 for hysteresis-free efficient flexible perovskite solar module," *Nature communications,* vol. 9, no. 1, p. 4609, 2018.

[39] F. Di Giacomo, H. Fledderus, H. Gorter, G. Kirchner, I. de Vries, I. Dogan, W. Verhees, V. Zardetto, M. Najafi, and D. Zhang, "Large area> 140 cm 2 perovskite solar modules made by sheet to sheet and roll to roll fabrication with 14.5% efficiency," in *2018 IEEE 7th World Conference on Photovoltaic Energy Conversion (WCPEC)(A Joint Conference of 45th IEEE PVSC, 28th PVSEC & 34th EU PVSEC)*, 2018: IEEE, pp. 2795-2798.

[40] U. Nations. "Sustainable Development Goals." https://sdgs.un.org/goals (accessed 27/06/2024.

Annex A - Efficiencies of PSC devices reported in literature according to the active area

Table An. A 1. PSC devices produced in ambient air conditions.

Device	Active area / cm^2	PCE / %	Year / Ref.
cell	0.09	15.20	2018/[26]
	0.10	12.70	2018/[27]
	0.10	21.80	2020/[17]
	0.13	14.50	2020/[28]
	0.30	12.30	2019/[7]
module	2.10	14.90	2022/[29]
	3.78	10.34	2020/[10]
	6.80	14.40	2020/[17]
	8.30	10.00	2018/[15]
	17.60	10.60	2017/[30]
	20.77	16.63	2021/[31]
	168.75	11.10	2018/[32]

Table An. A 2. PSC devices produced in a controlled atmosphere.

Device	Active area /cm^2	PCE / %	Year / Ref.
cell	0.01	18.30	2018/[33]
	0.06	18.00	2018/[34]
	0.09	22.70	2020/[35]
	0.16	20.80	2021/[36]
module	2.20	14.60	2021/[36]
	7.92	19.60	2020/[35]
	10.20	18.70	2020/[35]
	12.00	15.20	2021/[37]
	16.07	14.89	2018/[38]
	36.10	15.60	2019/[16]
	144.00	13.80	2018/[39]
	151.88	11.10	2018/[39]

Annex B - Sustainable Development Goals



Figure An. B. 1. Sustainable Development Goals.[40]

Appendix A – Set of experiments for PTAA and perovskite layer optimization

Table Ap. A. 1. Set of experiments to be performed according to JMP software and the results obtained for the first PTAA optimization.

Coating speed / $mm \cdot s^{-1}$	Slot-die plate temperature / ºC	Ink concentration / $mg \cdot mL^{-1}$	R^{-1} / Ω^{-1}
15	60	1.50	0.95
		2.00	1.1
	70	1.75	1.25
	80	1.50	1.14
		2.00	1.2
20	60	1.75	1.09
	70	1.50	1.28
		1.75	1.05
			1.24
		2.00	1.34
	80	1.75	1.19
25	60	1.50	1.24
		2.00	0.9
	70	1.75	1.03
	80	1.50	1.23

Table Ap. A. 2. Set of experiments to be performed according to JMP software and the results obtained for the second PTAA optimization.

Coating speed / mm·s^{-1}	Ink concentration / mg·mL^{-1}	Gap / µm	R^{-1} / Ω^{-1}
15	1.25	50	0.93
		200	0.00
	1.63	125	1.01
	2.00	50	1.11
		200	0.00
20	1.25	125	0.90
	1.63	50	1.06
		125	0.94
		200	0.00
	2.00	125	1.05
25	1.25	50	0.89
		200	0.00
	1.63	125	1.14
	2.00	50	1.01
		200	0.00

Table Ap. A. 3. Set of experiments to be performed according to JMP software and the results obtained for the perovskite optimization.

Coating speed / $mm \cdot s^{-1}$	Ink concentration / $mol \cdot L^{-1}$	Gap / µm	PCE / %
8	0.75	50	1.62
		125	4.81
		200	0.00
	1.00	125	6.59
	1.25	50	3.03
		125	4.38
		200	0.00
10	0.75	50	2.70
		125	0.13
	1.10	50	7.51
	1.25	50	6.71
16.5	0.75	125	1.93
	1.00	50	2.85
		125	2.72
			2.36
		200	0.00
	1.25	125	4.16
25	0.75	50	3.14
		125	0.10
		200	0.00
	1.00	50	5.00
	1.25	50	3.34
		200	0.00

Appendix B – Principal photovoltaic parameters of solar cells

Table Ap. B. 1. Principal photovoltaic parameters of full PSCs prepared with the selected deposition conditions of PTAA, under illumination of 1 sun (100 mW·cm^{-2}, AM 1.5, room temperature).

	V_{OC} / V	J_{SC} / mA·cm^{-2}	FF	PCE / %
Ink concentration: 2 mg·mL^{-1} Coating speed: 20 mm·s^{-1} Gap: 50 µm Slot-die plate temperature: 70 ºC	0.83	17.53	0.51	7.51
	0.83	18.81	0.46	7.19
	0.76	12.70	0.62	5.99
	0.83	18.09	0.43	6.45
	0.83	18.89	0.46	7.32
	0.86	17.29	0.40	5.93
	0.77	15.51	0.46	5.49
Ink concentration: 1.5 mg·mL^{-1} Coating speed: 21.66 mm·s^{-1} Gap: 50 µm Slot-die plate temperature: 70 ºC	0.84	15.62	0.43	5.68
	0.85	14.18	0.37	4.40
	0.83	16.18	0.49	6.67
	0.84	16.79	0.51	7.14
	0.77	13.46	0.60	6.21
Ink concentration: 1.89 mg·mL^{-1} Coating speed: 15 mm·s^{-1} Gap: 85 µm Slot-die plate temperature: 70 ºC	0.84	16.11	0.39	5.30
	0.81	16.43	0.45	5.99
	0.85	15.25	0.49	6.41
	0.76	16.82	0.39	4.98
	0.76	16.82	0.39	4.98

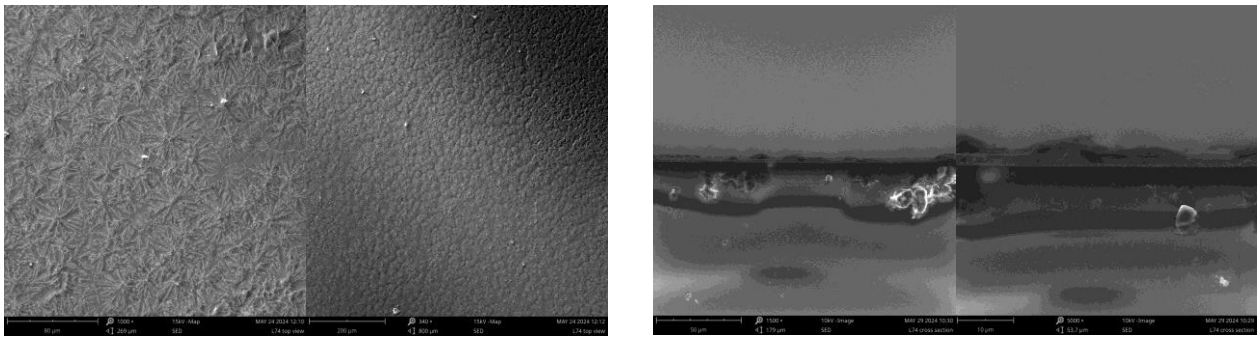
Table Ap. B. 2. Principal photovoltaic parameters of full PSCs prepared with the optimized deposition conditions of perovskite layer, under illumination of 1 sun (100 mW·cm^{-2}, AM 1.5, room temperature).

	V_{OC} / V	J_{SC} / mA· cm^{-2}	FF	PCE / %
Ink concentration: 1.1 mol·L^{-1} Coating speed: 8 mm·s^{-1} Gap: 65 µm Slot-die plate temperature: 70 ºC	0.84	17.39	0.44	6.49
	0.83	20.86	0.38	6.55
	0.84	18.88	0.46	7.32
	0.79	18.69	0.49	7.21
	0.87	16.21	0.37	5.27
	0.86	19.02	0.44	7.30
	0.80	17.73	0.36	5.13
	0.85	18.59	0.46	7.19
	0.81	18.63	0.44	6.62

Table Ap. B. 3. Principal photovoltaic parameters of full PSC devices and the segmented device prepared using the optimized PTAA and perovskite slot-die conditions.

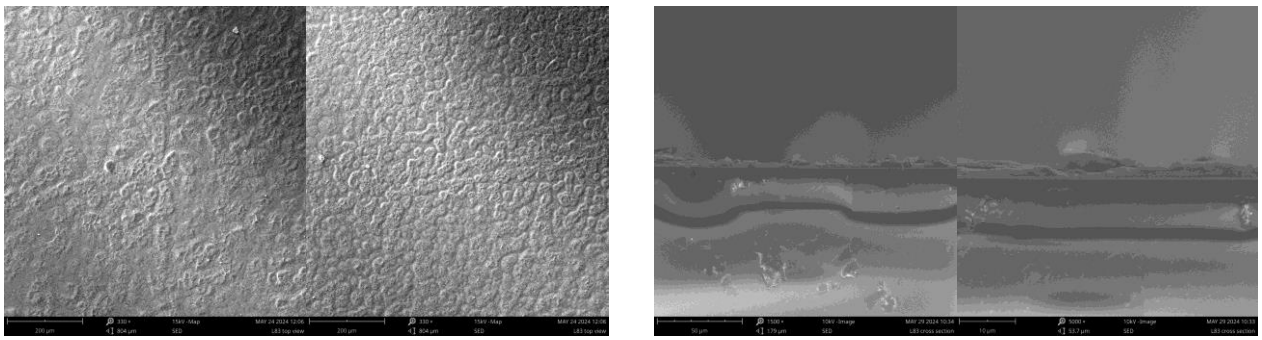
	V_{OC} / V	J_{SC} / mA·cm^{-2}	FF	PCE / %
5 cm^2	0.86	19.02	0.44	7.30
Zone 1	0.87	18.89	0.53	8.75
Zone 2	0.86	19.97	0.44	7.51
Zone 3	0.87	20.38	0.47	8.40

Appendix C – SEM images of the perovskite layer



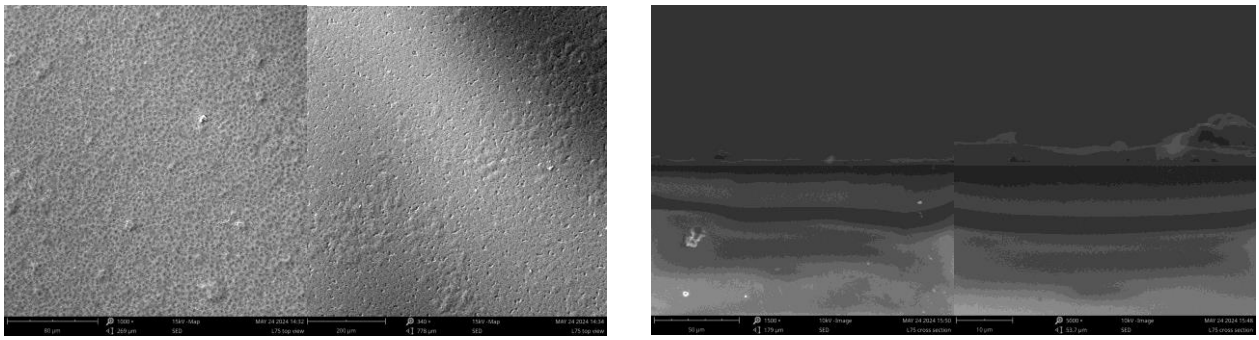
a) b)

Figure Ap. C. 1. SEM images: a) top-view, and b) cross-section (perovskite slot-die deposition conditions: 8 mm·s^{-1} coating speed, 0.75 mol·L^{-1} of perovskite solution concentration and 50 µm of gap).



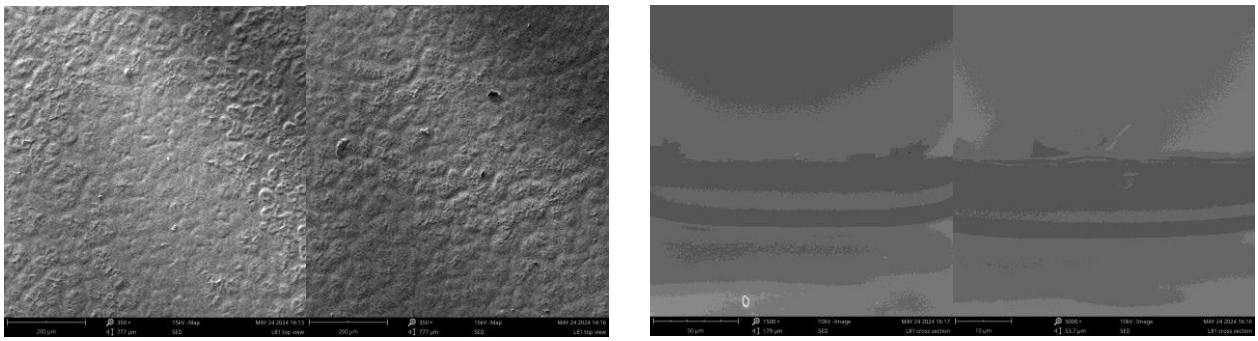
a) b)

Figure Ap. C. 2. SEM images: a) top-view, and b) cross-section (perovskite slot-die deposition conditions: 10 mm·s^{-1} coating speed, 0.75 mol·L^{-1} of perovskite solution concentration and 50 µm of gap).



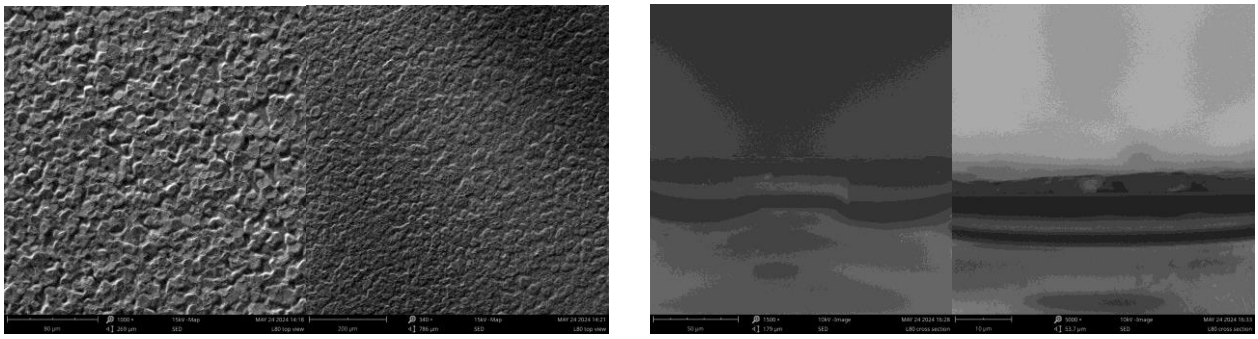
a) b)

Figure Ap. C. 3. SEM images: a) top-view, and b) cross-section (perovskite slot-die deposition conditions: 25 mm·s^{-1} coating speed, 0.75 mol·L^{-1} of perovskite solution concentration and 50 µm of gap).



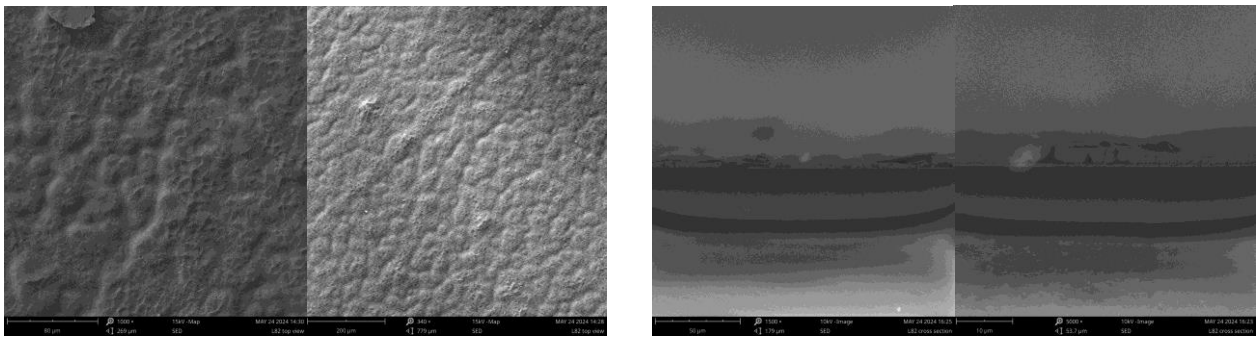
a) b)

Figure Ap. C. 4. SEM images: a) top-view, and b) cross-section (perovskite slot-die deposition conditions: 8 mm·s^{-1} coating speed, 0.75 mol·L^{-1} of perovskite solution concentration and 125 µm of gap).



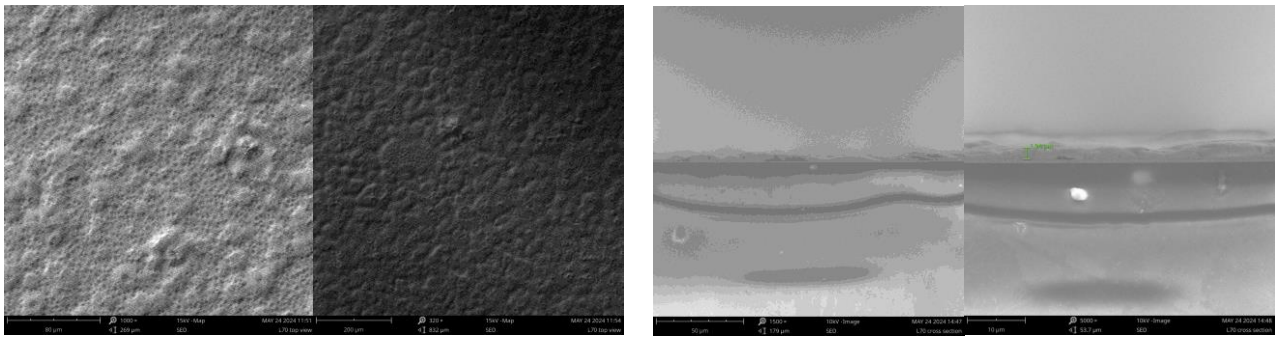
a) b)

Figure Ap. C. 5. SEM images: a) top-view, and b) cross-section (perovskite slot-die deposition conditions: 16.5 mm·s^{-1} coating speed, 0.75 mol·L^{-1} of perovskite solution concentration and 125 µm of gap).



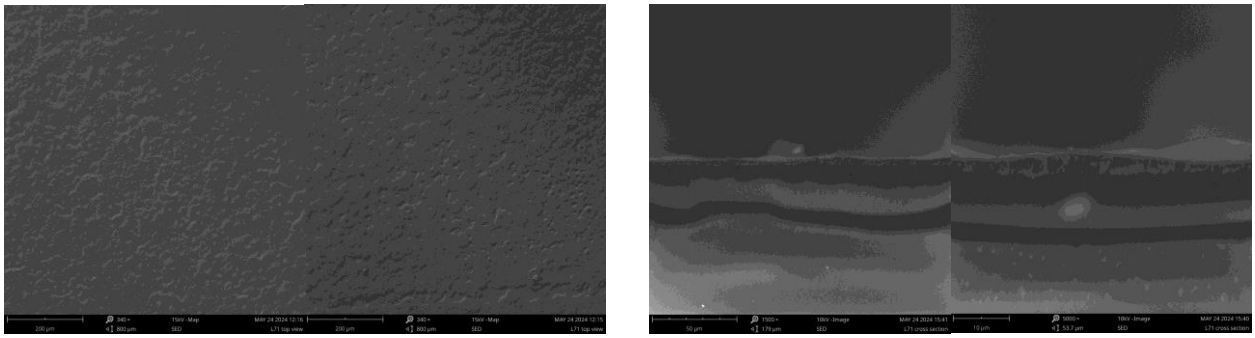
a) b)

Figure Ap. C. 6. SEM images: a) top-view, and b) cross-section (perovskite slot-die deposition conditions: 25 mm·s^{-1} coating speed, 0.75 mol·L^{-1} of perovskite solution concentration and 125 µm of gap).



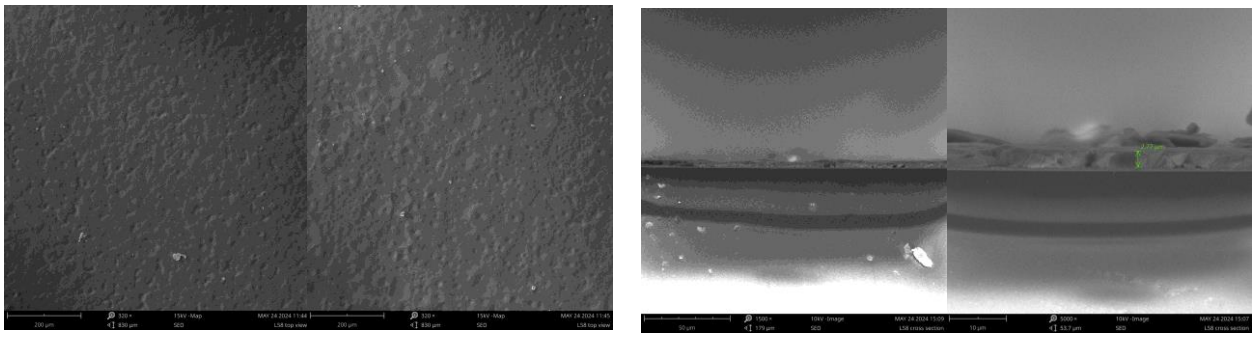
a) b)

Figure Ap. C. 7. SEM images: a) top-view, and b) cross-section (perovskite slot-die deposition conditions: 16.5 mm·s^{-1} coating speed, 1.00 mol·L^{-1} of perovskite solution concentration and 50 µm of gap).



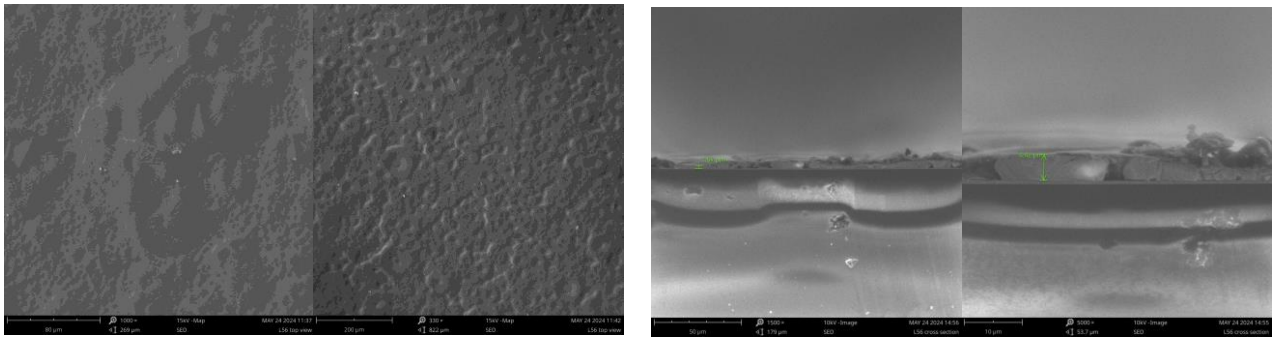
a) b)

Figure Ap. C. 8. SEM images: a) top-view, and b) cross-section (perovskite slot-die deposition conditions: 25 mm·s^{-1} coating speed, 1.00 mol·L^{-1} of perovskite solution concentration and 50 µm of gap).



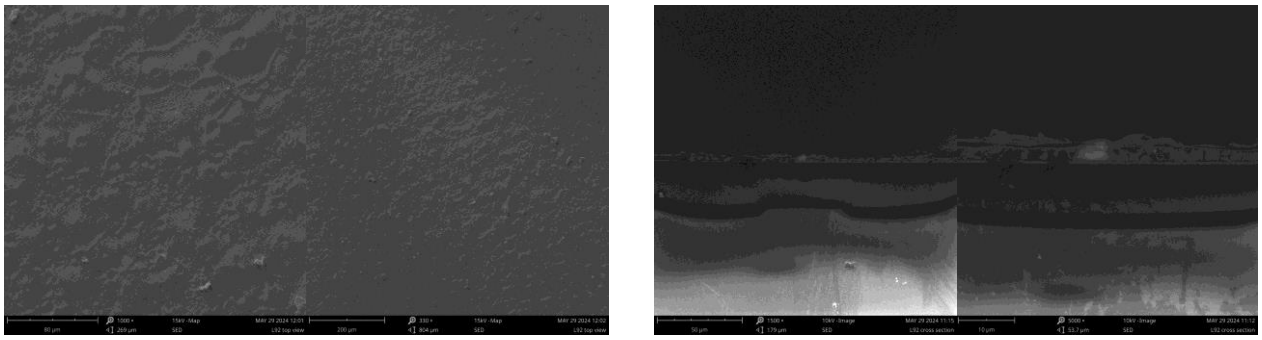
a) b)

Figure Ap. C. 9. SEM images: a) top-view, and b) cross-section (perovskite slot-die deposition conditions: 8 mm·s^{-1} coating speed, 1.00 mol·L^{-1} of perovskite solution concentration and 125 µm of gap).



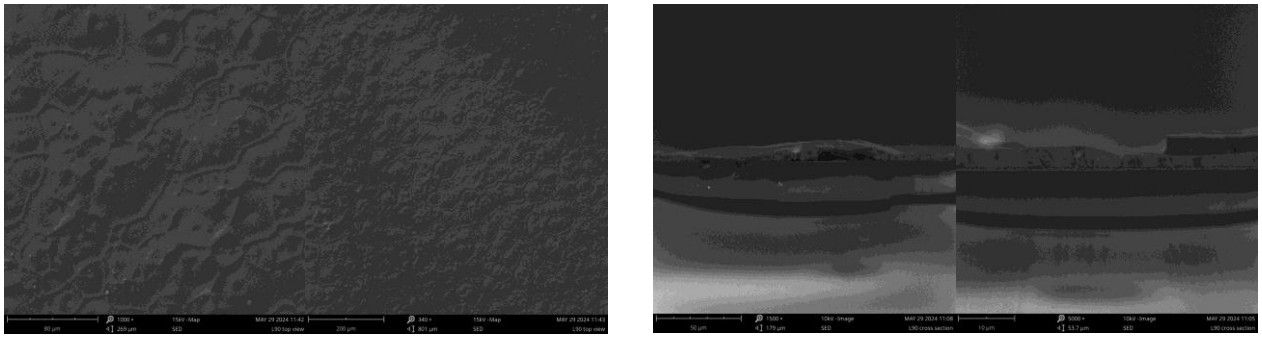
a) b)

Figure Ap. C. 10. SEM images: a) top-view, and b) cross-section (perovskite slot-die deposition conditions: 16.5 mm·s^{-1} coating speed, 1.00 mol·L^{-1} of perovskite solution concentration and 125 µm of gap).



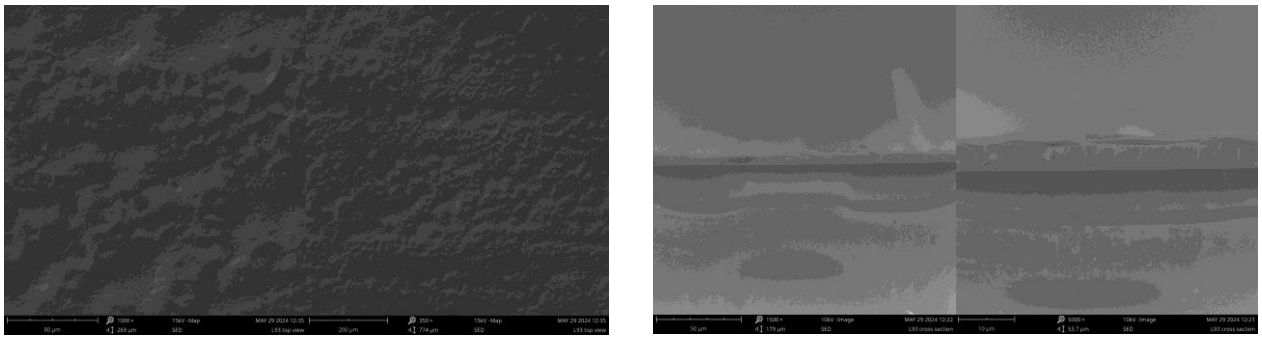
a) b)

Figure Ap. C. 11. SEM images: a) top-view, and b) cross-section (perovskite slot-die deposition conditions: 8 mm·s^{-1} coating speed, 1.25 mol·L^{-1} of perovskite solution concentration and 50 µm of gap).



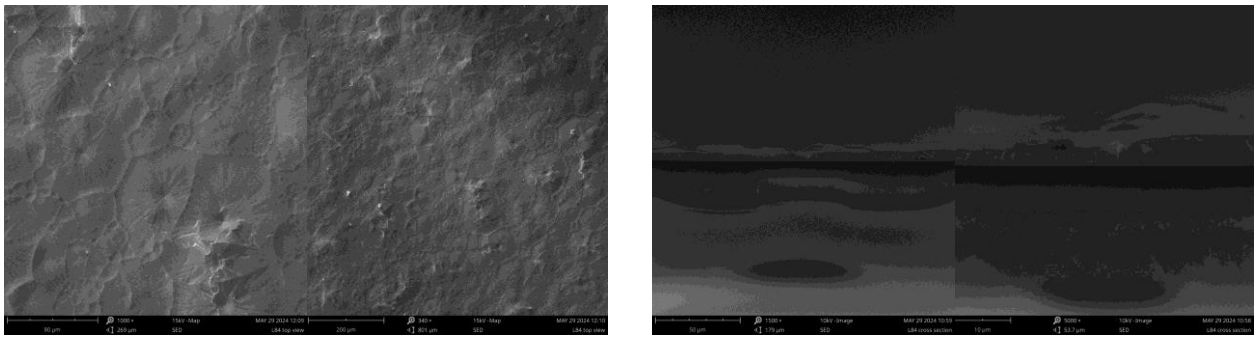
a) b)

Figure Ap. C. 12. SEM images: a) top-view, and b) cross-section (perovskite slot-die deposition conditions: 10 mm·s^{-1} coating speed, 1.25 mol·L^{-1} of perovskite solution concentration and 50 µm of gap).



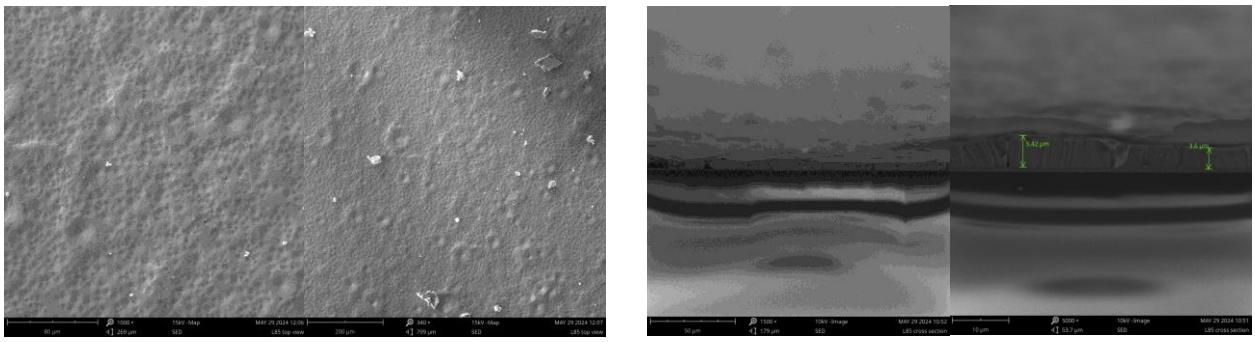
a) b)

Figure Ap. C. 13. SEM images: a) top-view, and b) cross-section (perovskite slot-die deposition conditions: 25 mm·s^{-1} coating speed, 1.25 mol·L^{-1} of perovskite solution concentration and 50 µm of gap).



a) b)

Figure Ap. C. 14. SEM images: a) top-view, and b) cross-section (perovskite slot-die deposition conditions: 8 mm·s^{-1} coating speed, 1.25 mol·L^{-1} of perovskite solution concentration and 125 µm of gap).



a) b)

Figure Ap. C. 15. SEM images: a) top-view, and b) cross-section (perovskite slot-die deposition conditions: 16.5 mm·s^{-1} coating speed, 1.25 mol·L^{-1} of perovskite solution concentration and 125 µm of gap).